Wageningen University

Master Thesis

Quantifying the SOA budget in the atmospheric boundary layer in southeastern United States

Author:

Juhi Nagori

Supervisors:

Ruud Janssen[1]

Jordi Vilà-Guerau de Arellano[2]

A thesis submitted in fulfilment of the requirements
for the degree of Master of Science

in the

Meteorology and Air Quality (MAQ)
Earth and Environment

May 2017

[1]Postdoctoral Associate, Department of Civil and Environmental Enginerring, MIT
[2]Personal Professor, Meteorology and Air Quality Section, Wageningen University

WAGENINGEN UNIVERSITY

Abstract

Meteorology and Air Quality (MAQ)
Master of Science

by Juhi Nagori

Secondary Organic Aerosol (SOA) is found in high quantities above southeastern United States. This SOA is formed by Biogenic Volatile Organic Compounds (BVOCs), with isoprene and monoterpenes being the major sources. Previous studies have analysed the gas-phase photochemistry of SOA formation and the chemical reactions that lead to SOA during the Southern Oxidant & Aerosol Study (SOAS). We utilise the mixed layer model (MXLCH-SOA) with an interactive land surface to calculate surface heat fluxes and BVOC emissions and to recreate the diurnal SOA evolution during the SOAS campaign. We represent a characteristic day constrained by comprehensive surface and upper air observations taken during the campaign. We study the formation of local SOA by using newly discovered chemical pathways: mainly to form isoprene hydroxy hydroperoxide SOA (ISOPOOH-SOA) and isoprene epoxydiol-derived SOA (IEPOX-SOA). We also attempt to distinguish between locally produced and non-locally produced SOA by separating SOA factors into aged SOA being advected to the site and freshly formed SOA, by using degree of oxidation as a proxy for age. In this coupled land-atmosphere system, we are able to represent well the surface energy balance above the canopy and the diurnal evolution of the boundary layer. The gas-phase chemistry is also represented well. The isoprene emissions are underestimated compared to direct flux observations though the isoprene mixing ratio is captured well by the model. The model presents differences compared to the observed SOA concentrations: The diurnal evolution of IEPOX-SOA and Low-Oxygenated Oxidized Organic Aerosol (LO-OOA) is not modelled well while the diurnal evolution of ISOPOOH-SOA is modelled satisfactorily. Based on the case study, we further explore the sensitivities of the model to both dynamical and chemical factors, namely entrainment, advection, cloud formation, and emission/deposition rates. We find that entrainment makes a large difference to the model and brings it closer to the observations; dry deposition and advection also need to be taken into account to improve the model. Lastly, we analyse the budget of SOA to evaluate the dynamical and chemical contributions to the SOA budget and find that background OA entrainment has the largest effect on SOA budget in the late morning; monoterpene SOA has the largest initial contribution (90%). IEPOX-SOA and ISOPOOH-SOA have an 80% and 3.7% contribution to the SOA budget respectively at the end of the day (16:00 CST).

Contents

Chapter 1

Introduction

Atmospheric aerosols alter the radiative budget, and hence climate, by absorption/scattering of radiation (Goldstein et al., 2009) and cloud formation (Novakov and Penner, 1993), lead to haze formation (Huang et al., 2014), can pose health risks to humans (Mauderly and Chow, 2008) and can affect boundary layer dynamics (Barbaro et al., 2014). Secondary organic aerosols (SOA) make up a sizeable fraction of the aerosol in the atmosphere (Murphy et al., 2006) and are formed from the oxidation of volatile organic compounds (VOCs) (Jimenez et al., 2009). A large fraction of SOA is formed through biogenic volatile organic compounds (BVOCs), especially isoprene and monoterpenes, which are emitted in large quantities from forested areas (Goldstein et al., 2009; Guenther et al., 1995). SOA makes up approximately 80-90% of total aerosol mass found in the southeastern US (Ahmadov et al., 2012; Stocker et al., 2013).

Many measurement campaigns have been carried out to measure SOA concentrations, including a series of studies done in southeastern US in 2013, collectively known as Southeast Atmosphere Studies (SAS) held over the period of 1 June to 15 July 2013 (Hidy et al., 2014). The SAS campaign coordinated comprehensive measurements of trace gas and aerosol compositions, aerosol physics and chemistry and meteorological dynamics across the southeastern US atop three ground sites, measurement towers, four aircrafts, sondes and a pre-exisitng network of surface and satellite measurements (Carlton et al., 2016). Southern Oxidant and Aerosol Study (SOAS), an intensive measurement campaign, part of the SAS, was performed near the Talladega forest in Centerville, Alabama, where a comprehensive dataset on oxidants, BVOCs, SOA and meteorological variables was collected (Xu et al., 2015a).

The diurnal evolution of SOA is driven by a myriad of factors. Firstly, the emissions of BVOCs, especially isoprene and monoterpenes, act as SOA precursors and their emissions depend on vegetation and meteorological dynamics (Guenther et al., 1995). These BVOCs, in this case isoprenes and monoterpenes, undergo chemical transformations in and just above the atmospheric

mixed layer including photooxidation of isoprene and oxidation of monoterpenes (Jimenez et al., 2009; Carlton et al., 2009) to form SOA through gas-particle (G/P) partitioning, reactive uptake and condensation of semi-volatile organic compounds (SVOCs) (Donahue et al., 2006; Krechmer et al., 2015; Gaston et al., 2014). The oxidant availability depends on nitrogen oxide (NO_x) regimes: ozone formation and OH recycling are affected by NO_x availability (Sillman et al., 1990; Trainer et al., 1987). The deposition of the BVOCs and SOA also affect the diurnal evolution of SOA (Nguyen et al., 2015a; Farmer et al., 2013). Lastly, boundary layer (BL) dynamics and the interaction between the BL and the free troposphere (FT) drive the diurnal SOA evolution (Janssen et al., 2012). Surface fluxes and entrainment of heat modulate the convective boundary layer (CBL) and, consequently, the mixing ratio of scalars (Van Heerwaarden et al., 2009), BVOCs (Vilà-Guerau de Arellano et al., 2009) and the SOA concentration (Janssen et al., 2012). Hence, to represent the diurnal SOA evolution accurately, we need to integrate the aforementioned factors that drive the SOA (Janssen et al., 2012, 2013) and BVOC diurnal evolution (Vilà-Guerau de Arellano et al., 2009, 2011).

In order to model the diurnal evolution of SOA and variations of SOA chemistry in the CBL over the SOAS measurement site, we use the mixed layer model (MXL), constrained by observations from the SAS datasets. MXL, developed by Lilly (1968) and Tennekes (1973), is a 0-dimensional model for the dynamics of the convective boundary layer (CBL) that assumes vigorous mixing throughout the BL; hence state variables and atmospheric constituents are constant with height throughout their evolution in the diurnal convective BL. Chemical transformations can be taken into account by introducing essential gas-phase reactions of the O_3-NO_x-VOC-HO_x system is added to the MXL model (Vilà-Guerau de Arellano et al., 2009). A SOA formation module, which uses the Volatility Basis Set (VBS) approach (Donahue et al., 2006), is also included as per Janssen et al. (2012); the resulting MXLCH-SOA model which couples the BL dynamics, the essential chemical reactions and SOA formation through G/P partitioning is henceforth used (Janssen et al., 2012).

However, Janssen et al. (2013) underestimated the SOA formation with G/P partitioning, and hence utilised a simple description of isoprene-SOA formation, suggesting the need for the addition of isoprene chemistry-related mechanisms that lead to SOA formation. Here, we add formulations for newly proposed pathways accounting for the reactive uptake and condensation to form isoprene-derived SOA to the model. These include reactions forming isoprene hydroxy hydroperoxides-derived SOA (ISOPOOH-SOA) and isoprene epoxydiol-derived SOA (IEPOX-SOA). Hu et al. (2016) describe in more detail IEPOX-SOA formation in low nitrogen dioxide (NO_2) conditions while Krechmer et al. (2015) discuss the formation of ISOPOOH-SOA, through condensation of Low Volatility Organic Compounds (LVOCs). IEPOX-SOA contributed around

15 to 30% to the total mass of SOA measured during the SOAS campaign due to low NO_2 conditions (Lopez-Hilfiker et al., 2016); the ISOPOOH-SOA contribution is considerably lower, though still significant at 3.3% of the global SOA (Krechmer et al., 2015). ISOPOOH is a precursor of both IEPOX-SOA and ISOPOOH-SOA, hence the formation of SOA factors by both reactive uptake and condensation is taken into account. Other mechanisms that have been recently discussed in literature include isoprene-SOA formed through the methacryloyl peroxynitrate (MPAN) pathway. However, this pathway, which is favoured under low temperatures and high NO_2 conditions, had a negligible contribution to SOA formation during the SOAS campaign (Nguyen et al., 2015a).

The gas-phase photooxidation chemistry of isoprene for the SOAS campaign was represented well in the MXLCH model, and a detailed evaluation of the main dynamics and chemistry of the BL was also included (Su et al., 2016). Based on Su et al. (2016)'s dynamical and gas-phase chemistry initial conditions, the diurnal BL dynamics and the gas-phase and SOA chemistry for representative day for the campaign was modeled in the MXLCH-SOA model. The main research aims of this study were:

1. Interactively calculating the surface heat fluxes in the model above the canopy; which were previously prescribed fluxes (Su et al., 2016). This couples the dynamics and chemistry of the model to the land surface; the sensitivity of the model and SOA formation to land surface variables, can then be studied and compared to the observations.

2. Interactively calculating the BVOC (isoprene and monoterpene) fluxes; which were also previously prescribed (Su et al., 2016). This couples the dynamics and chemistry of the model to the land surface variables and vegetation factors that affect BVOC emissions, and allows us to further explore of the effects of these variables on SOA formation.

3. Under these coupled conditions, modelling the diurnal mixed layer SOA evolution, constrained by tower and aircraft observations from SOAS and other SAS studies, using an updated chemical mechanism including G/P-partitioning and reactive uptake to account for formation of SOA.

4. As the model only accounts for locally produced SOA, distinguishing between and discussing the locally and non-locally produced SOA.

5. Exploring the sensitivity of the model (and hence SOA production), to 1) the deposition velocities (surface effect) of ISOPOOH and IEPOX, as they are considerable (3 cm/s) (Nguyen et al., 2015b); to 2) FT concentrations of ISOPOOH-SOA and IEPOX-SOA (entrainment effect); to 3) ventilation flux due to shallow cumulus and the consequent

mass flux effect (at top of BL effect); and to 4) to advection of SOA (long-range transport effect).

6. Evaluating the budget of the total SOA in order to break it down into contributions (deposition, entrainment and chemistry) of the different SOA components.

Chapter 2

Methodology

2.1 Measurements

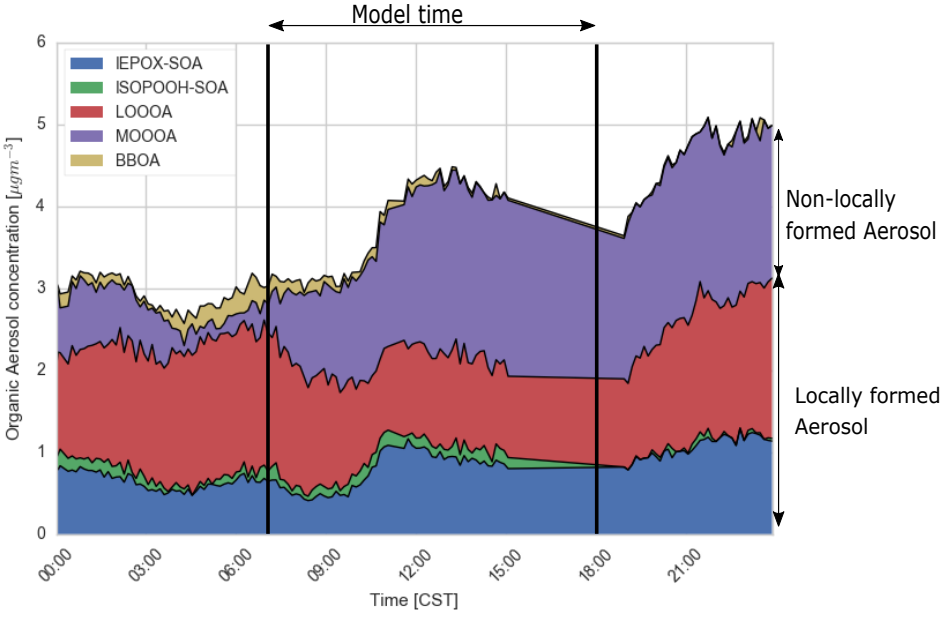

FIGURE 2.1: Observed diurnal evolution of secondary organic aerosols as a sum of biomass burning OA (BBOA), isoprene epoxydiol-derived SOA (IEPOX-SOA), isoprene hydroxyhydroperoxide SOA (ISOPOOH-SOA), more oxidized oxygenated OA (MOOOA) and low oxidised oxgenated OA (LOOOA) measured at the SOAS, Centerville site, which were distinguished into locally produced (blue, green and red, at the bottom) and non-locally produced (purple and yellow) organic aerosol (Discussed in Section 2.3.1). The area between the two black lines is the time modelled in the mixed layer model.

The SOAS campaign was conducted in the summer of 2013, and a comprehensive dataset on oxidants, Biogenic Volatile Organic Compounds (BVOCs), aerosols and other meteorological variables was collected (Xu et al., 2015a). The campaign aimed to understand the fundamental atmospheric processes above southeastern US by studying and measuring the coupled interactions between emissions, atmosphere-biosphere exchange, chemistry, aerosol processes, and

climate change (Carlton et al., 2016). The campaign comprised of two ground-based measurement sites: South-East Aerosol Research and Characterization (SEARCH) measurement tower near Brent and Centerville, Alabama and the Alabama Aquatic Biodiversity Center (AABC) flux tower (at 35m height) near Marion, Alabama, both of which measured in or above the mixed forest canopies (Su et al., 2016). Vertical profiles were plotted from measurements done by the Whole Air Sample Profiler (WASP) containing flights, NCAR-130 and NOAA P-3 aircrafts and a SENEX flight, which flew over the Centerville site on June 11^{th} between 11:00 - 12:00 CST.

Volatile Organic Compounds (VOC), in particular monoterpenes and isoprenes, eddy covariance fluxes (using 3-D wind component measurements) and heat fluxes were measured above the canopy atop the AABC tower (Su et al., 2016). WASP collected vertical profiles of VOCs; and the system (WASP) was integrated with a meteorological data sensor, taking measurements of ambient temperature, relative humidity, 3-D wind components and GPS data (Su et al., 2016).

Trace gas concentrations of ozone (O_3), nitrogen oxides (NO_x) and hydroxides (HO_x) and the boundary layer height were measured at the SEARCH site, while the NCAR-130 flight took airborne measurements of isoprene, monoterpenes, trace gases, photolysis rates, methyl vinyl ketone (MVK) and methacrolein (MACR), and other meteorological data (Su et al., 2016).

Secondary Organic Aerosol (SOA) was measured with an aerosol mass spectrometer (AMS) at the SEARCH site. Positive matrix factorization (PMF) analysis of the organic aerosol data was used to allocate the source of the organic aerosol (DeCarlo et al., 2006; Canagaratna et al., 2007) into biomass burning OA (BBOA), isoprene epoxydiol-derived SOA (IEPOX-SOA), isoprene hydroxyhydroperoxide SOA (ISOPOOH-SOA), more oxidized oxygenated OA (MOOOA) and low oxidised oxygenated OA (LOOOA) (Xu et al., 2015b), which are shown in Figure 2.1.

2.2 Designing a new model reference case

The mixed layer model (MXLCH), which couples dynamics and reduced gas-phase chemistry, essential reactions of O_3-NO_x-VOC-HO_x (van Stratum et al., 2014; Vilà-Guerau de Arellano et al., 2009) is used with a SOA formation module as per Janssen et al. (2013). The following assumptions are made to for the mixed layer model:

1. The MXLCH model assumes vigorous mixing throughout the convective boundary layer (CBL), hence mixing ratios in the mixed layer are constant with height (Stull, 1988).

2. The boundary layer height (h) grows due to entrainment, driven by the sensible and latent heat flux (Tennekes, 1973).

3. The atmospheric boundary layer (ABL) and the free troposphere (FT) are separated by a shallow inversion layer and scalars and variables are exchanged through entrainment between these layers (Tennekes and Driedonks, 1981).

4. Large-scale meteorology is prescribed as external forcings eg. mean vertical velocity, advection of heat, moisture and chemically reactive species (Su et al., 2016; Vilà-Guerau de Arellano et al., 2015).

2.2.1 Fundamental concepts

Assuming horizontal homogeneity, incompressibility and applying Reynold's decomposition (Bernard and Wallace, 2002), the one-dimensional conservation equation for a scalar, C, is calculated by the change in vertical flux of the scalar ($(\overline{w'C'})$) with height and the chemical transformation term (S_c).

$$\frac{\partial \langle C \rangle}{\partial t} = -\frac{\partial (\overline{w'C'})}{\partial z} + S_c \tag{2.1}$$

In a mixed layer, or the CBL, we vertically integrate conservation equations of heat, moisture, momentum, and reactants to get constant values with height, known as bulk/slab or mixed layer values, of potential temperature (θ), specific humidity (q), gas and solid reactants and wind speeds (u and v) (Indicated by triangular brackets $\langle\rangle$) (Lilly, 1968; Tennekes and Driedonks, 1981).

However, in order to solve Equation (2.1) in the mixed layer, we couple it to thermodynamic equations pertaining to the mixed layer evolution, as the evolution of a scalar in the mixed layer depends on the dynamics that drive the mixed layer (Stull, 1988; Vilà-Guerau de Arellano et al., 2009). Hence, to accurately depict the mixed layer evolution of a scalar, we also need to accurately calculate the growth of the mixed layer, and evolutions of heat, moisture and wind in the mixed layer. The mixed layer growth is quantified by the boundary layer (BL) height, h (in m). The mixed layer is topped by an inversion, above which is the FT, and the height of this inversion is the BL height, which is governed by the following equation:

$$\frac{\partial h}{\partial t} = -\frac{(\overline{w'\theta'_v})_e}{\Delta \theta_v} + w_s \tag{2.2}$$

The boundary layer growth, h, depends singularly on the introduction of heat in the system. The heat, in the form of the virtual potential temperature θ_v, is introduced by the entrainment flux, $(\overline{w'\theta'_v})_e$, which is the exchange of air, and consequently heat, between the BL and the FT, or the jump of θ_v at the top of the inversion, $\Delta\theta_v$; this is difference of θ_v between the ABL and

the FT, which is represented by a sharp discontinuity. θ_v is related to potential temperature (θ) and specific humidity (q), and it is the θ dry air would have to have the same density as moist air at the same pressure. The BL height also depends on w_s, which is the subsidence velocity, which depends on large-scale subsiding air motions. (Lilly, 1968; Tennekes, 1973; Stull, 1988; Vilà-Guerau de Arellano et al., 2009).

The evolution of h depends on the latent and sensible heat fluxes, as they drive the θ and q mixed layer evolution, and therefore the evolution of θ_v. These fluxes are commonly prescribed in the mixed layer model; however, these fluxes can be interactively calculated using a coupled land-surface scheme as is described in Section 2.2.2.

Hence, through vertical integration and addition of thermodynamic equations, the mixed layer scalar tendency is determined by:

$$\frac{\partial \langle C \rangle}{\partial t} = \frac{(\overline{w'C'})_s - (\overline{w'C'})_e - (\overline{w'C'})_M}{h} + S_c \tag{2.3}$$

which now depends on the surface flux of C ($(\overline{w'C'})_s$) in ppb m s^{-1} that can either represent emission or deposition fluxes. The deposition flux is related to the reactant mixing ratio and a deposition velocity of a species. Dry deposition acts as a loss term and reduces the mixing ratio and concentrations in BL that would be missed if only photochemical destruction alone was taken into account (Karl et al., 2009) The entrainment flux of C ($(\overline{w'C'})_e$), also in ppb m s^{-1}, depends on the entrainment velocity, w_e, and is the difference in concentration of SOA and its precursors (ΔC) in the FT and the ABL ($w_e \cdot (C_{FT} - \langle C \rangle)$). This jump for scalar usually manifests with a sharp discontinuity as observed in Figure 2.2. $(\overline{w'C'})_M$ (also in ppb m s^{-1}) is the ventilation flux, associated with mass flux, which results from fair weather clouds in the mixed layer. This ventilation flux is calculated in the model based on van Stratum et al. (2014), and are described in the Appendix .1. h is the boundary layer height (m) and S_c is the chemical transformation term.

Equation (2.3) can be used to specifically analyse the mixed layer evolution of SOA as the vertical profile of SOA (See Figure 2.2) is well-mixed for the representative day. However, the equation does not take into account horizontal transport of C.

The bulk mixed layer tendency of OA (in ppb s^{-1}), taking into account advection, is then calculated from Equation (2.4).

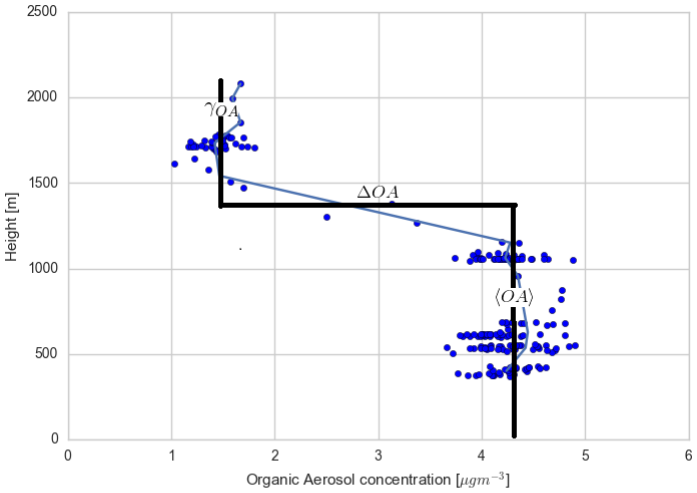

FIGURE 2.2: Measured vertical profile of organic aerosol (blue dots) taken during the SENEX campaign above the SOAS campaign sites on June 11, 2013 at 11:00 CST, averaged for different heights (blue line) and overlaid with a typical convective boundary layer; a mixed layer represented by a bulk value ($\langle OA \rangle$), a sharp discontinuity in the inversion layer (ΔOA) and a value in the free troposphere (γ_{OA})

.

$$\overbrace{\frac{\partial \langle OA \rangle}{\partial t}}^{\text{Tendency}} = \frac{\overbrace{(\overline{w'OA'})_s}^{\text{Surface flux}} - \overbrace{(\overline{w'OA'})_e}^{\text{Entrainment flux}} - \overbrace{(\overline{w'OA'})_M}^{\text{Ventilation flux}}}{h} + \overbrace{\left(-U_k \frac{\partial \langle OA \rangle}{\partial x_k}\right)}^{Advection} + \overbrace{S_{OA}}^{\text{SOA formation}} \tag{2.4}$$

For the surface and entrainment fluxes (in ppb m s^{-1}), we analyse the deposition and FT values. The deposition of ISOPOOH and IEPOX is analysed as a sensitivity analysis in Section 2.3.2. As the total SOA in the FT was measured by SENEX aircraft (Figure 2.2) we have an FT value for total SOA, however, the FT measurements of all components of SOA are not known; a sensitivity analysis for FT values of ISOPOOH-SOA and IEPOX-SOA is done in Section 2.3.2.

The ventilation flux ($(\overline{w'OA'})_M$ in ppb m s^{-1}) leads to a loss of SOA in the presence of shallow cumulus clouds which transport scalars from the mixed (sub-cloud) layer to the cloud layer due to mass flux (van Stratum et al., 2014). A sensitivity analysis of mass flux is done and we discuss the main components of this term that we have introduced in the mixed layer model in Appendix .1.

The advection term represents the horizontal advection of SOA into the mixed layer system. U_k represents the horizontal zonal (u) and meridional (v) winds (m s^{-1}) which transport SOA (ppb) in the horizontal (∂x_k in m) x and y directions. A sensitivity analysis of advection of SOA is done in Section 2.3.2.

The SOA formation term, S_{OA} (in ppb s^{-1}), is dependent on the production (P_{OA}) and loss (L_{OA}) terms that affect SOA formation.

$$S_{OA} = P_{OA} - L_{OA} \tag{2.5}$$

This term represents all the chemical reactions that encompass the SOA formation; the SOA formation from the VBS module and formation reactions of ISOPOOH-SOA and IEPOX-SOA. These reactions can be found in Table A.2, while more discussion on the SOA formation reactions is done in Section 2.2.4. The chemical reactions are also modulated by the precursors of SOA, mainly monoterpenes and isoprenes. Hence, the emissions of monoterpene and isoprene (precursors) are discussed in Section 2.2.3. A conceptual diagram summarises all the effects on the SOA tendency (Figure 2.3).

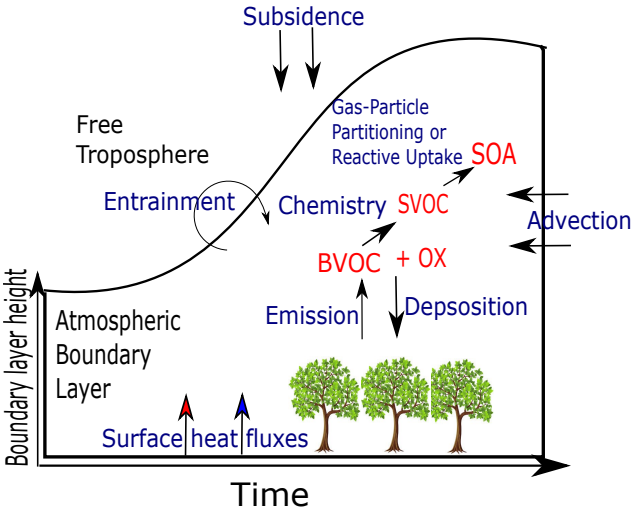

FIGURE 2.3: Schematic of the main processes (blue) in the boundary layer, dynamic and chemical, that affect the Secondary Organic Aerosol budget above the SOAS campaign site, with the mixing ratios of the scalars in red.

The evolution of the jump of SOA (ppb s^{-1}) at the inversion is calculated from the free tropospheric lapse rate of SOA (γ_{OA} in ppb m^{-1}), the boundary layer growth evolution (m s^{-1}), the subsidence velocity (m s^{-1}), the bulk layer tendency of OA (ppb s^{-1}) and the SOA transformation term in the FT ($S_{OA_{FT}}$ in ppb).

$$\frac{\partial \Delta OA}{\partial t} = \gamma_{OA}\left(\frac{\partial h}{\partial t} - w_s\right) - \frac{\partial \langle OA \rangle}{\partial t} + S_{OA_{FT}} \tag{2.6}$$

2.2.2 Interactive surface fluxes

Su et al. (2016) prescribed the surface moisture and heat fluxes with sinusoidal functions that were fitted with eddy covariance flux data at AABC, to simulate the diurnal flux function

(Figure 2.5) in the MXLCH model. In contrast, we interactively calculate the surface moisture and heat fluxes in the MXLCH-SOA model following the representation.

The latent and sensible heat flux are calculated using the Penman-Monteith equations as per Van Heerwaarden et al. (2009).

TABLE 2.1: Advanced surface variables: plant and soil initial and boundary layer conditions to study the effect of a coupled land-atmosphere scheme. The plant scheme has been taken from Van Heerwaarden et al. (2009)'s value for the broad leaf trees.

Property	Value	Units
Initial surface (skin) temperature (T_s)	298	K
Soil moisture (wg)	0.40	$m^3 m^{-3}$
Soil moisture deeper soil layer (w2)	0.34	$m^3 m^{-3}$
Wilting point (wwilt)	0.29	m^3 m^{-3}
Volumetric water content field capacity (wfc)	0.44	m^3 m^{-3}
Saturated volumetric water content (wsat)	0.55	m^3 m^{-3}
CL* parameter a	0.083	[-]
CL* parameter b	11.4	[-]
CL* parameter c	12.0	[-]
Coefficient force term moisture (C1sat)	0.342	[-]
Coefficient restore term moisture (C2ref)	0.3	[-]
VPD correction factor for r_s (gD)	0.03	[-]
Transpiration resistance ($r_{s;min}$)	200	s m^{-1}
Soil transpiration resistance ($r_{soil;min}$)	20	s m^{-1}
Leaf Area Index (LAI)	5	$m^2 m^{-2}$
Vegetation fraction c_{veg}	0.9	[-]
Initial temperature top soil layer	286	K
Temperature deeper soil layer (T2)	285	K
Thermal conductivity skin layer divided by depth (Λ)	20	W m^{-2} K^{-1}
Roughness length momentum (z_{om})	1.4	m
Roughness length heat (z_{oh})	1.4	m

*Clapp and Hornberger retention curve parameter

Table 2.1 shows the surface characteristics used to calculate the dynamic fluxes interactively, where typical values for broadleaf trees are used. Figure 2.5 shows the modelled (interactively) dynamic fluxes compared to the observations at the AABC flux tower. The model does not include a wind module, however, the initial U-wind and V-wind are set at 0.01 m/s. This initial value is set at higher than 0 since the aerodynamical resistance r_a is proportional to the convective velocity scale, w_*. In the first time step, the w_* is too small and hence in order to calculate the r_a for this time step, the initial u and v are set at 0.01 m/s.

2.2.3 Interactive BVOC Emissions

Su et al. (2016) also prescribed the BVOC (terpene and isoprene) fluxes with a sinusoidal function fitted to BVOC emissions measured at the AABC tower. BVOC emissions from plants are dependent on meteorological and vegetation factors (Guenther et al., 1995) and are calculated in the mixed layer model interactively for this research.

To interactively calculate the isoprene emissions in the mixed layer model we used the Model of Emissions of Gases and Aerosols from Nature (MEGAN), from Guenther (2006). In this model, the emissions, E, of isoprene, and other BVOCs, are parametrized by:

$$E = [\epsilon][\gamma][\rho] \tag{2.7}$$

$[\epsilon]$ are the base emissions in μ g $m^{-2}hr^{-1}$ of compound, while ρ accounts for the production and loss of the BVOC within canopy, which, for isoprene, is set to 0.96 (Guenther, 2006). The base emission rates are dependent on the plant functional type, and since we are over a broadleaf forest the emission rate for isoprene is set at 3000 $\mu g m^{-2} h^{-1}$ (=0.83 $\mu g m^{-2} s^{-1}$); though it is low for a broad-leaf area it is used as it is able to reproduce the isoprene mixing ratio observations. γ (unitless) represents emission activity factors, and for isoprene is given by:

$$\gamma = \gamma_{CE} \times \gamma_{Age} \times \gamma_{SM} \tag{2.8}$$

γ is a lumped correction factor (Wang et al., 2017); it takes into account effect of the canopy environment γ_{CE}, the leaf age γ_{Age} and soil moisture γ_{SM}.

A constant value for γ_{Age} is used ($\gamma_{Age} = 1$). In order to calculate the γ_{CE}, we utilise the parametrized canopy environment emission activity (PCEEA) algorithm. This is calculated by:

$$\gamma_{CE} = \gamma_T \times \gamma_P \times \gamma_{LAI} \tag{2.9}$$

The γ's are activity factors that are dependent on variations of temperature, light and the leaf area (Guenther, 2006); γ_T is temperature dependent, γ_{LAI} is dependent on the leaf area index while γ_P is dependent on the leaf-level photosynthetic photon flux density (PPFD) in $\mu mol m^{-2} s^{-1}$, which is related to the photosynthetically active radiation (PAR). The PAR depends on the incoming solar radiation and is the radiation that organisms can use for photosynthesis.

Isoprene emission respond to changes in PPFD at canopy-level by:

$$\gamma_P = 0 \qquad a < 0, a > 180 \tag{2.10a}$$

$$\gamma_P = \sin(a)[2.46(1 + 0.0005 \cdot (P_{daily} - 400))\phi \cdot 0.9\phi^2] \qquad 0 < a < 180 \tag{2.10b}$$

where a is the solar angle (calculated by subtracting the zenith angle from 90 degrees) in degrees. P_{daily} is related to the PAR (multiplied by a conversion factor (4.766) to convert it from W/m^2 to μ mol $m^{-2}s^{-1}$) and represents the daily mean of the above canopy PPFD , and ϕ is the transmission of the above canopy PPFD which is non-dimensional (Guenther, 2006) and approximated by:

$$\phi = P_{ac}/(\sin(a)P_{toa}) \tag{2.11}$$

here P_{ac}, the above canopy PPFD, is also approximated from PAR multiplied by a conversion factor (4.766 - Based on GEOS-Chem Model). P_{toa}, the top of the atmosphere PPFD (Guenther, 2006), depends on the day of the year (DOY) as per:

$$P_{toa} = 3000 + 99 \cdot \cos(2 \cdot 3.14 \cdot (DOY - 10)/365) \tag{2.12}$$

The response of isoprene emissions to temperature is calculated by:

$$\gamma_T = E_{opt} \times [C_{T2} \times exp(C_{T1} \times x/(C_{T2} - C_{T1} \times (1 - exp(C_{T2} \times x)))] \tag{2.13}$$

Here $x = [(1/T_{opt}) - (1/T]/0.00831$, C_{T1} (=80) and C_{T2} (=200) are empirically derived coefficients, T_{opt} is the optimal temperature at which E_{opt} is calculated (Guenther, 2006):

$$T_{opt} = 313 + (0.6 \times (T_{daily} - 297) \tag{2.14}$$

$$E_{opt} = 1.75 \times exp(0.08 \times (T_{daily} - 297)) \tag{2.15}$$

where T_{daily} is the representative daily average air temperature at canopy level for the modelling period (K) which is set to 298K, based on surrounding temperature measured at the SOAS campaign site. Lastly, for canopy-level, the isoprene emission dependence on the leaf area index (LAI in m^3m^{-3}) variations is estimated by:

$$\gamma_{LAI} = 0.49LAI/[(1 + 0.2LAI^2)^{0.5}] \tag{2.16}$$

The last γ factor, γ_{SM}, is 1 if the soil moisture, θ is greater than θ_l; 0 if θ is less than the wilting point, θ_w, and $(\theta - \theta_w)/\Delta\theta_l$ if θ_w is less than θ which is less than θ_l; $\Delta\theta_l$ is an empirical parameter equalling 0.06 (Guenther, 2006).

TABLE 2.2: MEGAN parameters and values used in the mixed layer model

Property	Value	Units
ϵ_{Iso}	3000*(=0.83)	$\mu g m^{-2} hr^{-1} (s^{-1})$
ρ_{Iso}	0.96	[-]
γ_{Age}	1	[-]
γ_{SM}	1	[-]
Soil moisture (θ)	0.40	$m^3 m^{-3}$
Wilting point (θ_w)	0.29	$m^3 m^{-3}$
LAI	5	$m^3 m^{-3}$
P_{daily} and P_{ac}	(PAR** $\times$4.766)	$\mu mol m^{-2} s^{-1}$
C_{T1}	80	[-]
C_{T2}	200	[-]
T_{daily}	298	K
ϵ_{MT}	850* (=0.24)	$\mu g m^{-2} hr^{-1} (s^{-1})$
ρ_{MT}	1	[-]
β_{MT}	0.13	K^{-1}
T_s	298 (initial value)	K
T_{ref}	303	K

*Values used to fit the model to the isoprene (and monoterpene) mixing ratio observations
**Photosynthetically active radiation in Wm^{-2}, plotted in Figure 13

For the monoterpene flux, in Equation (2.7), the $\rho = 1$, $\epsilon = 850\ \mu g m^{-2} h^{-1}$ to fit the monoterpene mixing ratio observations and γ is given by:

$$\gamma = \gamma_{CE} \times \gamma_{SM} \tag{2.17}$$

As above, it is dependent on the canopy emission activity factor and the soil moisture emission activity factor. The soil moisture emission factor is 1. The canopy emission activity factor is calculated by:

$$\gamma_{CE} = \gamma_{LAI} \times \gamma_T \tag{2.18}$$

which depends on the LAI emission activity factor and the temperature emission activity factor. The γ_{LAI} is also 1, however the temperature emission activity factor is given by:

$$\gamma_T = exp(\beta_{MT} \times (T_s - T_{ref}) \tag{2.19}$$

Here β_{MT} is the beta (an empirical coefficient) for monoterpene, set at 0.13 K^{-1} (Sakulyanontvittaya et al., 2008), T_s is the skin temperature and T_{ref} is the reference temperature for BVOC Base Emission Rate (K) and equals 303 K. Table 2.2 summarises the parameters used to run this model. Figures depicting the γ factors are shown in Appendix .2.

2.2.4 Secondary Organic Aerosol Formation

Secondary organic aerosols (SOA) result from gas/particle (G/P) partitioning of semi-volatile organic compounds (SVOCs) or from reactive uptake of certain OVOC (oxidised VOCs) species on pre-existing aerosol. A reduced gas-phase scheme that leads to SOA formation is used as per Janssen et al. (2013) and Su et al. (2016). The SOA formation module utilises the Volatility Basis Set (VBS) approach from Donahue et al. (2006), which lumps semi-volatile products of VOC-oxidation into 4 bins of effective saturation concentration and partitioning is considered to be instantaneous. The 4 bins are logarithmically spaced and comprise a relevant range of product vapour pressures at 298K (Lane et al., 2008). The VBS module calculates the gas/particle partitioning per time step with the equation:

$$C_{OA} = \sum_i (X_{p,i} C_i) + OA_{bg} \quad ; \quad X_{p,i} = \left(1 + \frac{C_i^*}{C_{OA}}\right)^{-1} \tag{2.20}$$

C_{OA} is the concentration of SOA, which is converted from mixing ratio of SOA (in ppb) to concentration of SOA (in μgm^{-3} using a molar mass of 250 g mol^{-1}), $X_{p,i}$ is the fraction of compound i in aerosol phase (dimensionless). OA_{BG} is the background SOA, which is the total SOA in the system which includes advected SOA (assumed to be 3.2 μgm^{-3} based on total SOA observations, see Figure 2.1). We then subtract the advected SOA from the bulk SOA to evaluate specifically the SOA formed in the model, i.e. locally formed SOA. C_i^* is the effective saturation concentration of i, also in μgm^{-3}.

As the SOA formation using the VBS approach in Janssen et al. (2013) did not include all SOA precursors, new chemical mechanisms leading to SOA formation are added in this study. Therefore, in addition to Janssen et al. (2013) and Su et al. (2016)'s gas-phase reduced scheme and VBS reactions, reactions for IEPOX-SOA and ISOPOOH-SOA formation are added. IEPOX-SOA measured at this site contributed between 15 and 30% of SOA in the southeastern US (Lopez-Hilfiker et al., 2016), and ISOPOOH-SOA contributed 2.3% (Krechmer et al., 2015). As IEPOX-SOA is only considered to contribute to half of isoprene SOA formed, ISOPOOH-SOA

is presented as one of the contributors of isoprene SOA by Krechmer et al. (2015). The reactions for IEPOX-SOA and ISOPOOH-SOA formation are derived from Hu et al. (2016). The complete chemical reaction scheme can be seen in Table 5. Reactions 9, 16, 32-36 are added/altered to update the reaction mechanism.

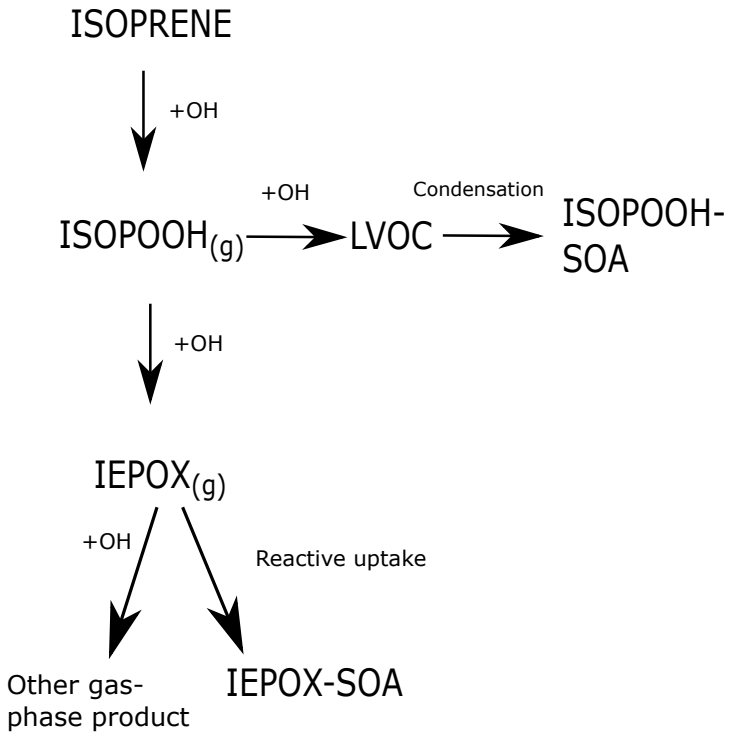

FIGURE 2.4: Chemical mechanism of IEPOX-SOA and ISOPOOH-SOA formed from the oxidation of isoprene (Hu et al., 2016). The g subscript denotes gas and LVOC is the low volatile organic compound.

The following changes were done to Hu et al. (2016)'s reaction scheme, for this research:

1. Hu et al. (2016) do not utilise temperature-dependent reaction rates. Hence, temperature-dependent reactions rates for reactions 9, 32, 34 (Paulot et al., 2009; Janssen et al., 2013) are utilised. For the other reactions, the temperature-dependent rates were not available in literature.

2. The photolysis reaction of IEPOX was removed as it is not observed under ambient conditions, but only in chamber reactions (Hu et al., 2016).

3. A yield for the IEPOX-SOA forming reaction, from IEPOX to IEPOX-SOA of 11% was added as per Hu et al. (2016) (R36).

4. A 4% yield for the ISOPOOH-SOA forming reaction was also added as per Krechmer et al. (2015) (R35).

5. In an attempt to prevent double-counting of SOA formed through the low-NO_x pathway, the following reaction is included: $IRO_2 + NO \rightarrow$ CiI which uses the Volatility Basis

Set from Janssen et al. (2013), which sorts the CiI into 4 bins based on their effective saturation concentrations (R16). High NO_x yields are used for CiI.

6. The reaction rate for IEPOX to IEPOX-SOA of 1.54e^{-4} s^{-1} is utilised (R36) (Hu et al., 2016).

2.3 Case Study

The 11th of June is used for the SOA observations (due to the availability of vertical profile measurements) and modelled as the representative day. This day was within the first intensive measurement period for the campaign and was characterised by winds predominantly from the West-Southwest and South-Southwest (10-12th of June) (Carlton et al., 2016). The day also recorded high temperatures and little precipitation (Carlton et al., 2016). The chemistry is initialized with the essential reactions from the O_3-NO_x-VOC-HO_x scheme and ISOPOOH-SOA and IEPOX-SOA forming reactions are added (See Table 5).

The model is constrained by observations from the SOAS campaign and the FT values for SOA are obtained from the SENEX flight that passed over Centerville site. To model a characteristic day, averaged values of variables (meteorological and gas-phase) from low-cloud cover days in the campaign (5, 6, 8, 10-13 June) are used to initialise the MXLCH model (Su et al., 2016). The dynamical conditions are initialized as per Table 3 and the chemical initial conditions are as per Table 4.

2.3.1 Local vs Non-local Aerosol Formation

Since we can only model local SOA, a distinction between local and non-local SOA needs to be made. Local SOA consists of any SOA that has been produced in the horizontally homogeneous footprint size of the model and is not being transported into this area by large-scale forcing (mainly advection). Hence, it is the area around the SOAS measurement site. BBOA is considered non-local as its concentration is a regional signal for the entire southeastern US (Washenfelder et al., 2015). A distinction between fresh and aged aerosol can be made; LO-OOA is assumed to be fresh as it has a low O:C ratio and thus has been less oxidised, while MO-OOA is assumed to be more aged as it has a high O:C ratio and has been oxidised more as it has been in the atmosphere longer (Xu et al., 2015b). However, MO-OOA could also result from extremely rapid oxidation in the system and hence could also be locally produced.

In order to allocate the MO-OOA, we analyse backward trajectories of air masses from the SOAS SEARCH site going back 48 hours using the NOAA Hysplit Trajectory Model at 100 m height

using the National Centers for Environmental Prediction (NCEP) Global Data Assimilation System half degree model. The trajectories started every 4 hours. The trajectories are then superimposed on land use data from the National Land Cover Database (NLCD) 2011.

2.3.2 Research Strategy

In order to study the sensitivity of the model to both dynamical and surface factors, the sensitivity analysis of SOA formation to entrainment, advection, cloud formation, and deposition velocity is carried out.

The model takes into account dry deposition, which acts as a loss of chemical species from the ABL to the surface. The deposition velocity, along with the chemical reactivity and transport, determines the lifetime of chemical species in the ABL, and acts as a loss term of said chemical species in the ABL.

A sensitivity analysis is done using dry deposition velocities of ISOPOOH and IEPOX from Nguyen et al. (2015b) of 3 cm/s (=0.03m/s). The first sensitivity analysis is done with a constant deposition flux for ISOPOOH and IEPOX at 0.03 m/s. A second sensitivity analysis is done with a sinusoidal function with 0.03 m/s as the maximum value at noon to show a diurnal cycle of the deposition flux, as in Nguyen et al. (2015b).

Though the total SOA concentration in the FT is known, the separate values of the different SOA factors in the FT are not known. These values are important to determine the jump between the FT and the ABL, in order to represent entrainment well. To study the effect of the FT concentrations in the model, the first sensitivity run is done with uniform values of all the SOA terms (Background OA, ISOPOOH-SOA and IEPOX-SOA). The second sensitivity analysis is done with the FT values of background SOA from the SENEX measurements, and the ISOPOOH-SOA and IEPOX-SOA FT values at 1/20 than that of the ABL (based on personal communication with Jose-Luis Jimenez).

Since the observations chosen are taken from cloudless days, the ventilation flux is not needed to calculate the budget of SOA. However, a sensitivity analysis is performed to analyse the effect of cloud formation on the SOA concentration. To study the influence of shallow cumulus clouds, we introduce a parametrization of the mass flux to account for cloud formation. As the control run/reference run has a very low cloud core fraction, to force the system to have a larger cloud fraction we set the γ_θ from 0.003 K m $^{-1}$ to 0.001 K m $^{-1}$, and start the cloud module two hours into the simulation.

Advection of aerosols introduces (reduces) aerosol in (out of) the system. Horizontal advection, which is a sum of advection from x and y directions, can be introduced in both the ABL and the

FT. The sensitivity analysis focuses on BL advection of SOA, and two runs with different values are carried out (0.000005 ppb m/s or 0.016 ppb/hr and 0.000001 ppb m/s or 0.0036 ppb/hr). The values were chosen to be small to see the effect that relatively low levels of advection had on the SOA diurnal evolution.

2.4 Budget Analysis

Equation (2.4) shows the different factors that contribute to the tendency of SOA. In order to analyse the contribution of different processes that lead to SOA formation from gas-phase processes, we calculate the SOA budget. The total budget of SOA, however, depends on 2 different budgets: the budget of monoterpene SOA and the budget of isoprene SOA. The monoterpene SOA in MXLCH is formed entirely through the VBS module while the isoprene SOA is formed through the VBS module and reactive uptake of IEPOX-SOA and condensation of ISOPOOH-SOA.

To allocate the contribution of chemistry for SOA formation, we first calculate the budget for SOA precursors. VOC's from biogenic emissions are the first SOA precursors; we can see the diurnal evolution of VOC based on the evolution of boundary layer dynamics. The VOC budget is as follows:

$$\frac{d\langle VOC\rangle}{dt} = \overbrace{\frac{F_{VOC}}{h}}^{\text{Emissions}} + \overbrace{\frac{w_e \Delta VOC}{h}}^{\text{Entrainment}} - \overbrace{\sum_j k_j \langle VOC\rangle \langle OX_j\rangle}^{\text{Chemistry}} + \overbrace{\left(-U_k \frac{\partial \langle VOC\rangle}{\partial x_k}\right)}^{\text{Advection}} \tag{2.21}$$

F_{VOC} represents the VOC emission flux (in ppb m s^{-1}), ΔVOC is the jump in the mixing ratio of VOC at the entrainment zone (in ppb), $\langle VOC\rangle$ is the mixed layer tendency of the BVOC (either monoterpene or isoprene in ppb) and $\langle OX_j\rangle$ is the mixing ratio of the oxidant (ppb) that reacts with the VOC to form SVOC. k_j is the reaction rate of the aforementioned chemical reactions; U_k is the horizontal wind speed (m s^{-1}) and $\partial\langle$VOC$\rangle$ is the mixing ratio difference (ppb) of the VOC in the horizontal ∂x_k (m)(Janssen et al., 2013).

The tendency of C_i, which represents SVOC (an intermediate SOA precursor), is very similar to the previous equation, but with no emission term. It depends on entrainment, the chemical reactions, advection and the deposition of the species. C_i also represents ISOPOOH and IEPOX in the following equation.

$$\frac{d\langle C_i\rangle}{dt} = \overbrace{\frac{w_e \Delta C_i}{h}}^{\text{Entrainment}} + \overbrace{\sum_j \alpha_i k_j \langle VOC\rangle \langle OX_j\rangle}^{\text{Chemistry}} + \overbrace{\left(-U_k \frac{\partial \langle C_i\rangle}{\partial x_k}\right)}^{\text{Advection}} - \overbrace{\frac{V_{dCi}\langle C_i\rangle}{h}}^{\text{Deposition}} \tag{2.22}$$

where ΔC_i is the jump at the inversion (ppb); $\partial\langle C_i\rangle$ is horizontal concentration difference (ppb) and V_{dCi} is the deposition velocity (m s^{-1}) for C_i. A constant deposition velocity of 2.4 cm s^{-1} for G/P partitioning of SVOCs is used (Janssen et al., 2013), while the one for ISOPOOH and IEPOX is also not taken into account as only the reference case budget is analysed.

The VBS-SOA tendency depends on the G/P-partitioning of the SVOCs (Janssen et al., 2013).

$$\frac{d\text{VBS-SOA}}{dt} = \sum_i \left[X_{p,i} \frac{dC_i}{dt} + C_i \frac{dX_{p,i}}{dt} \right] \tag{2.23}$$

$X_{p,i}$ is the fraction of compound i in aerosol phase (dimensionless) and C_i is the effective saturation concentration of i, in $\mu g m^{-3}$ (Donahue et al., 2006).

The ISOPOOH-SOA and IEPOX-SOA (collectively called ISOA) budget is:

$$\frac{d\text{ISOA}}{dt} = \overbrace{\frac{w_e \Delta ISOA}{h}}^{\text{Entrainment}} + \overbrace{\sum_j k_j \langle ISOA \rangle}^{\text{Chemistry}} + \overbrace{\left(-U_k \frac{\partial ISOA}{\partial x_k} \right)}^{\text{Advection}} - \overbrace{\frac{V_{dISOA} \langle ISOA \rangle}{h}}^{\text{Deposition}} \tag{2.24}$$

As ISOPOOH-SOA is formed through condensation of LVOC and IEPOX-SOA is formed from reactive uptake of IEPOX onto acidic aerosols, the chemistry only takes into account the reaction rates of these processes and the mixing ratio of the resulting SOA.

The total SOA budget is described by the entrainment of background OA, the tendency terms of the different SOA, the advection of SOA and the deposition of SOA.

$$\frac{d\langle OA \rangle}{dt} = \overbrace{\frac{w_e \Delta OA_{bg}}{h}}^{OA_{bg}\text{entrainment}} + \overbrace{\frac{d\text{VBS-SOA}}{dt} + \frac{d\text{ISOA}}{dt}}^{\text{SOA formation}} + \overbrace{\left(-U_k \frac{\partial OA}{\partial x_k} \right)}^{\text{Advection}} - \overbrace{\frac{V_{dOA} \langle OA \rangle}{h}}^{\text{Deposition}} \tag{2.25}$$

where ΔOA_{bg} is the jump in the background organic aerosol concentration between the BL and the FT (μg m^{-3}); $\partial\langle$OA$\rangle$ the horizontal concentration difference of SOA (μgm^{-3}).

We include advection in the equations for completeness, however, we do not take into account advection in the reference case as we do not include long-lived, non-locally produced aerosols, though a budget for the sensitivity analysis of advection would include an advection term. We also do not take into account the deposition flux of SOA, which according to Farmer et al. (2013) is quite small at approximately 0.02 $\mu g m^{-2} s^{-1}$, and so has been neglected.

The total SOA budget is then calculated by the 4 different chemical pathways/precursors (monoterpene-SOA, isoprene(VBS)-SOA, ISOPOOH-SOA and IEPOX-SOA).

Results & Discussion

2.5 Model evaluation

2.5.1 Surface fluxes and emissions

The surface heat fluxes and BVOC emissions were calculated interactively. Figure 2.5 shows the modelled and the observed surface fluxes measured at AABC's eddy covariance (EC) tower. The model was started at 07:00 CST (instead of 06:00 CST in Su et al. (2016)), a few hours after sunrise (which is at 04:30), to have a positive sensible heat flux, and to ensure that the assumption of a well-mixed BL is valid, as is discussed in Section 2.2.1

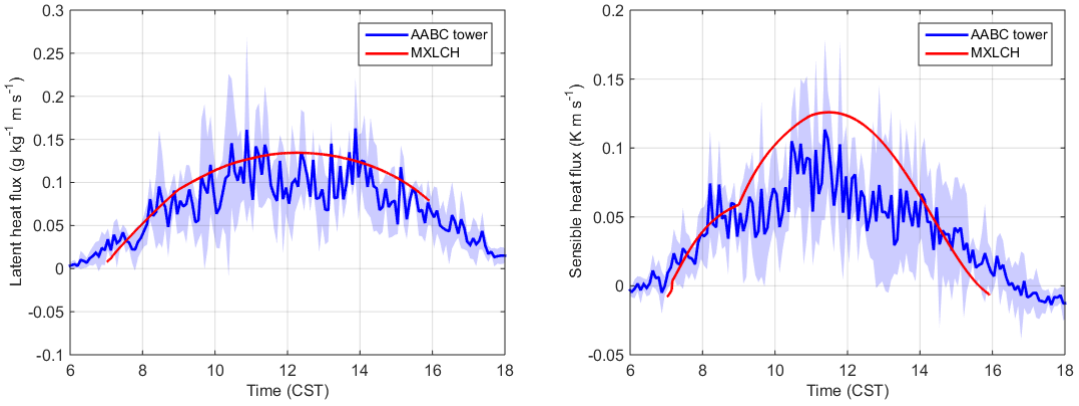

(A) Latent Heat Flux (B) Sensible Heat Flux

FIGURE 2.5: The modelled (red) and observed (blue) latent (a) and sensible (b) heat flux measured at the AABC flux tower on June 11, 2013 for the SOAS campaign.

The interactively calculated surface fluxes were able to represent the observed surface fluxes. The modelled latent heat flux peaked at noon, at 0.14 g kg^{-1} m s^{-1} and agreed well with the observations, since they both had a similar diurnal evolution (See Figure 2.5a). The modelled sensible heat flux peaked at 11:30 CST at 0.13 K m s^{-1}, which was higher (by approximately 18%) than the average observations (See Figure 2.5b). The sensible heat flux reaches 0 by 15:30, while the latent heat flux does not. EC measurements for sensible and latent heat fluxes have

an uncertainty of 15-20% thus, despite the 18% overestimation (at its peak) in the sensible heat flux, the model agrees well with the observations (Weaver, 1990; Field et al., 1992). Moreover, despite the overestimation of the model compared to the mean observations, the model generally falls in the range of observations.

The interactively calculated emission fluxes of isoprene were underestimated compared to the observations (See Figure 2.6a) However, Figure 2.7a, which is discussed later, shows that the modelled isoprene mixing ratio agrees well with the measurements and the modelled fluxes are close to the prescribed fluxes used by Su et al. (2016). The modelled monoterpene emission flux agrees with the observed monoterpene emission flux between 07:00 CST to 14:30 CST, after which they are overestimated. The isoprene and monoterpene emissions peak around noon. Isoprene emissions depend on PAR which also peak at midday, hence affecting the isoprene evolution. Temperatures are also high at noon, which also drive up emissions of isoprene and monoterpenes.

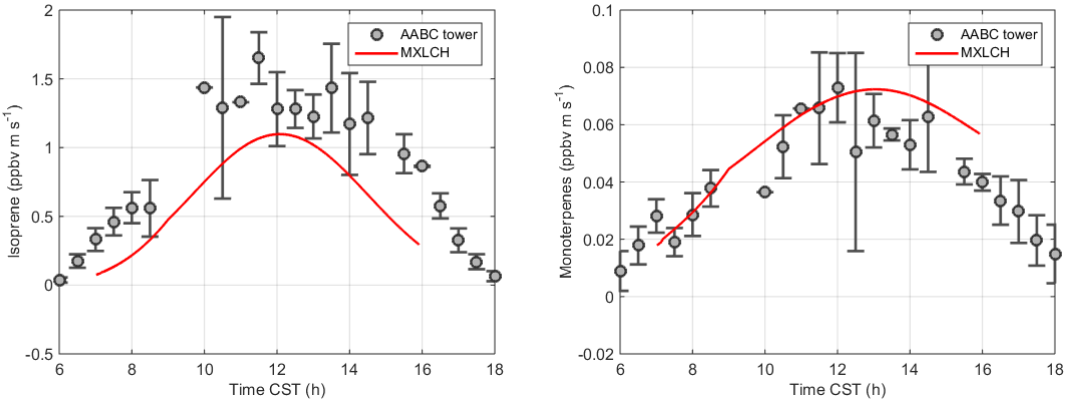

(A) Isoprene Flux (B) Terpene flux

FIGURE 2.6: a) Isoprene and b) Monoterpene fluxes modeled versus observations (measured at the AABC flux tower). The red line uses the MEGAN to calculate the BVOC fluxes.

MEGAN utilises Equation (2.7) to calculate the isoprene and monoterpene emission fluxes. The base emission rate for isoprene is set to 3000 $\mu gm^{-2}h^{-1}$, which is low for a region covered by broad-leaf trees (Guenther et al., 2012). The γ factors are also higher than calculated at the SOAS site (Alex Guenther, personal communication). The canopy temperature needs to be driven by air temperature instead of skin temperature, which has been done here, while the P_{daily} needs to be lowered (Situ et al., 2014). The conversion factor used to convert PAR to PPFD (4.766) was based on the conversion used in the GEOS-Chem (Goddard Earth Observing System - Chemistry) model. A conversion factor of 4.5 should be used instead, as it is more appropriate for direct/beam light (Alex Guenther, personal communication). This will be addressed in future research.

2.5.2 Diurnal cycle of VOC's and SOA

Figure 2.7 shows the diurnal evolution of modelled and measured isoprene, monoterpene and secondary organic aerosol (SOA). We observe a build-up of isoprene in the mixed layer throughout the day (from 0.5 ppb to 3.5 ppb), which is due to the increase in isoprene emissions observed during the day (Figure 2.6a). The isoprene mixing ratio is constant once the emissions of isoprene decrease (after 14:00 CST). This indicates a balance between emission and detrainment and chemistry. It agrees well with the observations, though it is slightly overestimated between 12:00 CST and 14:00 CST. The diurnal evolution of monoterpenes (See Figure 2.7b), shows a decrease in the mixing ratio of monoterpenes, with an initial mixing ratio of 1.2 ppb, which decreases to 0.3 ppb by 10:00 CST, after which it rises slightly (to 0.33 ppb at 16:00 CST). The decline of monoterpenes can be attributed to entrainment, that dilutes the monoterpene mixing ratio in the BL.

The diurnal evolution of SOA concentration, however, presents large differences when compared to the observations (Figure 2.7c). The sharp drop in the observed SOA in the morning (between 07:00 CST and 09:00 CST) is not well reproduced by the model, though the modelled SOA concentration does decrease around 2 hours after the model starts; this drop is due to entrainment. The increase in observed SOA after 10:00 is also missed, which could be due to the inability of the model to represent a more realistic γ_{SOA} profile in the free troposphere. It could also be due to SOA formation of a factor that peaks in this time period, or due to advection of SOA at that time. As we discuss later, the IEPOX-SOA formation peaks and there is advection at the measurement site in this time period; the advected SOA (MOOOA) increases between 10:00 and 12:00. This could affect SOA formation, especially SOA formed due to G/P partitioning in the model. At the end of the model run, the model overestimates the SOA concentration (2.2 μgm^{-3} compared to 1.9 μgm^{-3} observed at 15:30 CST). The increase in SOA concentration in the early afternoon are attributed to the addition of the new SOA formation pathways, which is discussed later in the total budget of SOA (See Figure 2.12). It is also possible that the modelled SOA lags behind SOA observations by 2 hours due to the sensitivity of isoprene and SOA to the boundary layer growth. As the dynamical observations are averaged over a few days, if the modelled boundary layer is shallower than the boundary layer that evolved on the 11^{th}, the time taken for the shallow boundary layer to grow will be longer, entrainment will be lagged, and thus the dilution of SOA concentrations seen in the observations as the boundary layer grows are delayed in the model. Moreover, there is a possibility that high concentrations of night-time SOA in the residual layer, which persists until noon (Wagner et al., 2015), could be affecting the entrainment flux. LO-OOA peaks during night-time (Ayres et al., 2015), and its persistence in residual layer is discussed below. The budget (See Figure 2.12) shows the contribution of entrainment, which is dependent on the FT concentration and profile of SOA,

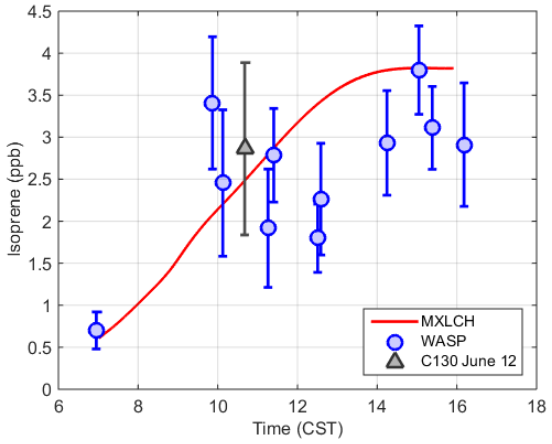

(A) Isoprene

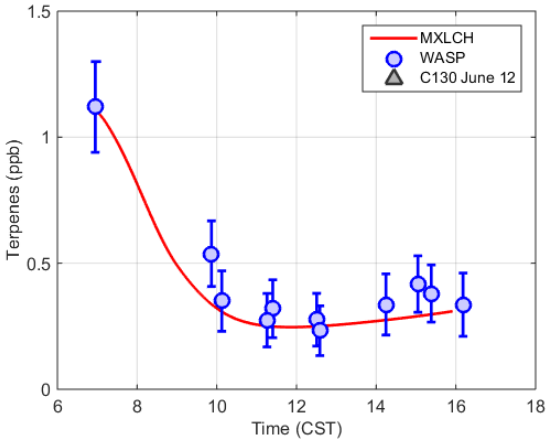

(B) Monoterpenes

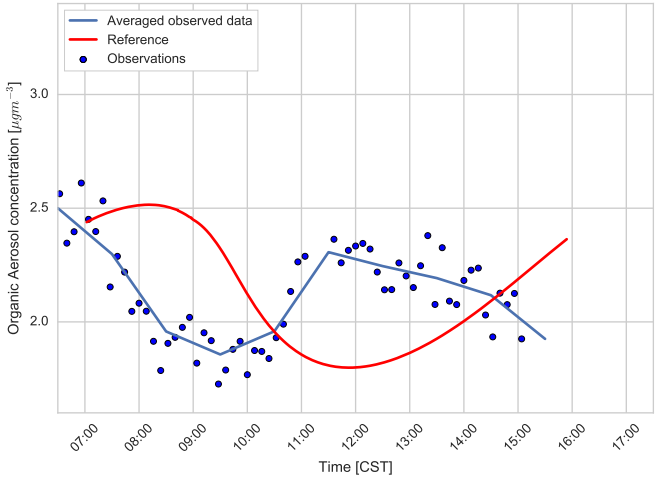

(C) Secondary organic aerosol

FIGURE 2.7: Measured (blue) and modelled (red) (a) mixing ratio of isoprene and (b) monoterpenes and (c) the concentration of SOA in the mixed layer at the Centerville SOAS site for June 11, 2013.

is approximately 80-90% in the late-morning to noon, this profile and concentration is quite important for the diurnal evolution of SOA.

In order to systematically pinpoint why the model fails to represent the daily evolution of SOA, we analyse the diurnal evolution of ISOPOOH-SOA, IEPOX-SOA and LO-OOA (Figure 2.8). These SOA factors are measured by aerosol mass spectrometer and allocated by positive matrix factorization (Xu et al., 2015b). The diurnal evolution of ISOPOOH-SOA is modelled well when compared to the observations: the modelled concentration increases slowly as the day progresses (0.10 to 0.15 μ g m^{-3} by 16:00). The model is unable to capture the diurnal evolution of IEPOX-SOA which is characterised by a peak in observations in the early afternoon, that is also missed in the total SOA diurnal evolution. Dry deposition is not taken into account for both IEPOX-SOA and ISOPOOH-SOA, while uniform concentrations of both SOA factors are

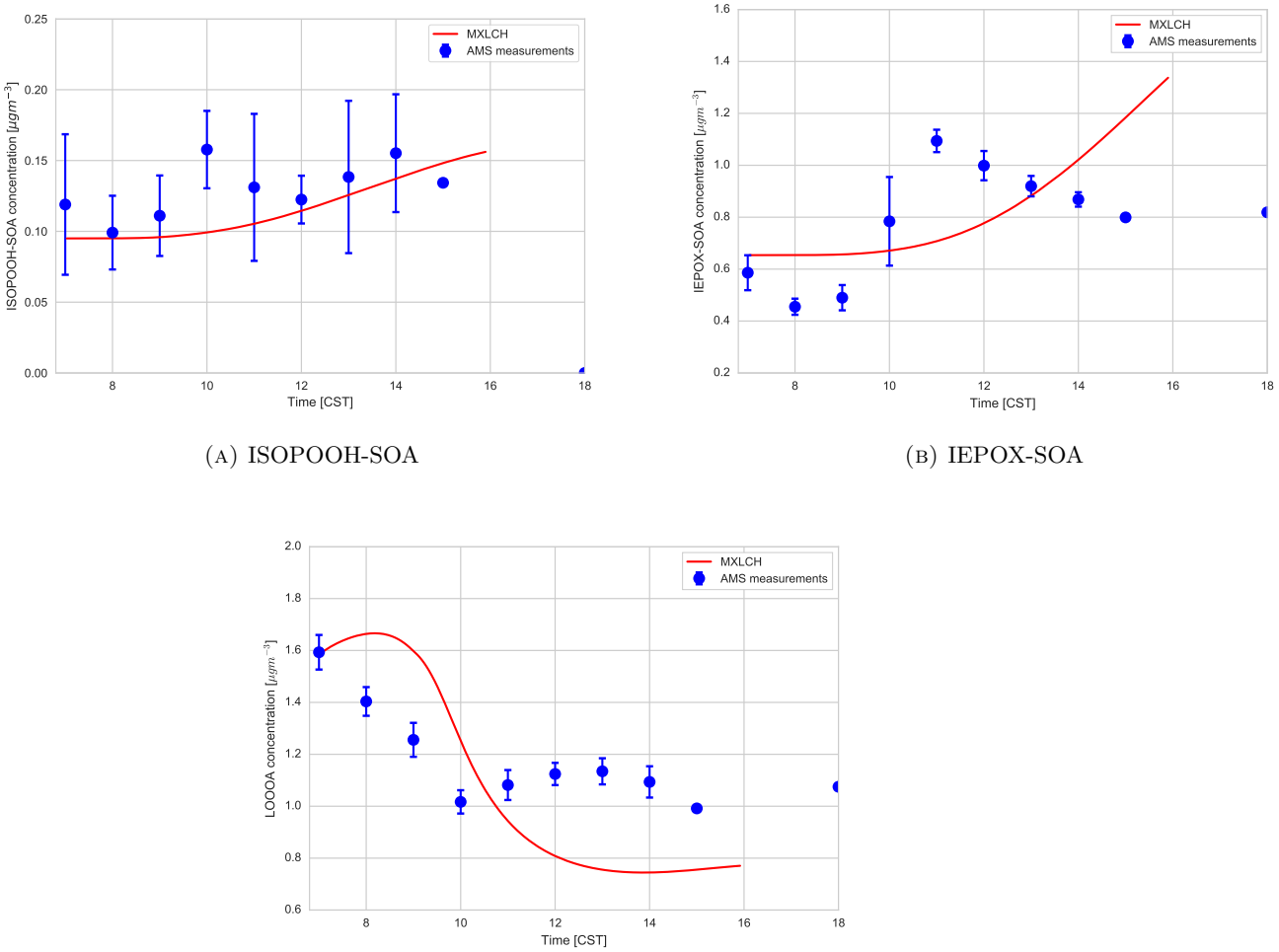

(A) ISOPOOH-SOA

(B) IEPOX-SOA

(C) LOOOA

FIGURE 2.8: The measured (blue) versus modelled (red, mixed layer model) (a) ISOPOOH-SOA, (b) IEPOX-SOA and (c) LO-OOA (the VBS-SOA in the model) at the Centerville SOAS site for June 11, 2013. The data was averaged per hours and the errorbars indicate the standard deviations.

used in the BL and FT. The initial drop in observed IEPOX-SOA, which is missed by the model, can be attributed to entrainment and is missed by the model due to the uniform concentration of IEPOX-SOA in the BL and FT. The IEPOX-SOA concentration is overestimated by the model (1.2 μ g m^{-3} at 15:00 CST) compared to the observations (0.8 μ g m^{-3} at 15:00 CST). This may be due to the FT concentration and profile of IEPOX-SOA. Since IEPOX-SOA is formed through reactive uptake of aerosol on acidic surfaces, the formation of IEPOX-SOA also depends on pH (Hu et al., 2016) and aerosol acidity (Gaston et al., 2014). Acidic sulphate aerosols, and therefore the diurnal evolution of sulphates (Xu et al., 2015b) and advection of sulphate aerosols (Lin et al., 2013), could affect the diurnal evolution of IEPOX-SOA. However, as pH dependency and advection are not taken into account, this remains an open issue.

As the diurnal evolution of both ISOPOOH-SOA and IEPOX-SOA do not show the sharp

decrease in SOA concentration in the morning, which is observed in the total SOA observations, we look at the diurnal evolution of LO-OOA. Figure 2.8c shows the observed and modelled LO-OOA. There is a sharp decrease in observed LO-OOA between 07:00 CST and 10:00 CST. LO-OOA in the model is attained from G/P partitioning of isoprene and monoterpene SOA (through the VBS module) and is mainly thought to consist of monoterpene-SOA in southeasternern US (Xu et al., 2015b). There is a decrease in the LO-OOA concentration due to the decrease in the monoterpene mixing ratio during the day, which is discussed in the budget. The modelled LO-OOA decreases from 1.6 to 0.8 μg m^{-3}, though it increases slightly during the first hour of the simulation. This rapid decrease in observed LO-OOA concentration in the early hours of the morning is not captured by the model. This could be due to the shallow boundary layer in these hours, or, since LO-OOA is a lumped term of monoterpene-derived SOA and isoprene-derived SOA, hence a loss term for one of the SOA factors could be missing. The underestimation of the afternoon SOA concentration (Figure 2.7) is mainly caused by the modelled LO-OOA, which is underestimated from 11:00 CST until the end of the simulation. G/P partitioning efficiency increases with increase in aerosol, as new aerosol condenses onto pre-existing aerosol (Janssen et al., 2012; Donahue et al., 2006), leading to an increase in aerosol formation. The partitioning efficiency is also favoured at lower temperatures (Takekawa et al., 2003). The observations show an increase in advected SOA (MOOOA) in the late morning, which is not taken into account in the model. Hence, the observed LO-OOA could be rising due to increased aerosol surfaces provided by advection, which increases G/P partitioning efficiency and more aerosol formation. Moreover, the FT profile of LO-OOA is not represented and we assume one concentration to describe the LO-OOA concentration in the FT which has an effect on the afternoon LO-OOA evolution. The difference between the modelled and observed LO-OOA in the late morning is also exacerbated by the steep decline in modelled LO-OOA due to entrainment, which is steeper than the decline in LO-OOA concentration in the early morning. LO-OOA peaks during night-time (Ayres et al., 2015), due to nitrate reaction with monoterpenes in the residual layer (Ayres et al., 2015), which could decouple from the surface layer and the nocturnal boundary layer, which removes surface influences like deposition (Li et al., 2014). This would increase the LO-OOA concentration in the residual layer, which could affect the entrainment flux. This would make the decrease in LO-OOA concentration in the mixed layer less pronounced, which could mean higher LO-OOA concentrations in the mixed layer around noon. The vertical profile of LO-OOA is not known, while the SOA vertical profile (Figure 2.2) measurements were taken between 11:00 CST and 12 CST, when the residual layer is almost dissipated (part of the well mixed layer). In Figure 2.2, there is a slight increase in concentrations of SOA between 500 and 1000 m, which could indicate the persistence of this residual layer, though the temperature is likely lower at 1000m than 500m which increases SOA formation as G/P partitioning efficiency is higher at lower temperatures (Takekawa et al., 2003). However, Janssen et al. (2012) noted

not accounting for the difference in temperature with height has a relatively small error in G/P partitioning efficiency.

2.6 Local vs non-local aerosol formation

In this section we distinguish the locally-formed SOA from non-locally formed SOA that is advected to the measurement site by mesoscale or synoptic pheonoemna. This separation is important as the model only accounts for locally-formed SOA. So far we have used observations of SOA as the sum of observed ISOPOOH-SOA, IEPOX-SOA and LO-OOA as we consider only these three factors to be locally-produced. The SOA measured at Centerville was composed of ISOPOOH-SOA, IEPOX-SOA, LO-OOA, MO-OOA and BBOA (See Section 2.1).

LO-OOA and isoprene-derived SOA were declared local in previous studies: back-trajectory analysis of LO-OOA and Isoprene-SOA was done by Xu et al. (2015b) and they concluded that both LO-OOA and Isoprene-SOA were locally produced. Isoprene has a short lifetime (1.4 h) and isoprene emissions are high at the measurement site, leading to high local isoprene-SOA production; the diurnal variability of LO-OOA did not change despite changing air masses and thus was apportioned as local SOA as well (Xu et al., 2015b). BBOA made up a small fraction of the total SOA mass measured at SOAS and was consistent with brown carbon and levoglucosan emitted during biomass combustion (Washenfelder et al., 2015). MO-OOA is aged aerosol that has undergone multiple cycles of oxidation in the atmosphere and hence is identified by a high atomic O:C ratio (Xu et al., 2015b; Washenfelder et al., 2015); it is usually considered to be long-range transport SOA though it could be locally produced with fast oxidation cycles.

In order to classify BBOA and MO-OOA, air mass trajectories were analysed. To determine the air mass origin we analyse back trajectories (going back 48 hours) arriving at the SOAS campaign site and the land use these air masses traverse. The complete trajectories were constructed using the NOAA Hysplit Trajectory model and can be seen in the Appendix (Figure 16). Figure 16 shows that air masses arriving at the site are predominantly from the South. The backward trajectories extend up to Florida and Cuba in the last 48 hours. Figure 2.9 zooms in on the land use the trajectories cross once they are over land. Multiple trajectories, some going back 48 hours at 100m, are passing areas of forest on their way to the measurement sites, and so are likely advecting SOA produced over these forests to the SOAS measurement site.

Washenfelder et al. (2015) and Budisulistiorini et al. (2015) posit that the MO-OOA and the BBOA represent the regional footprint of SOA in southeastern US. Washenfelder et al. (2015) compared the LV-OOA (low-volatility oxygenated organic aerosol; which are also more oxygenated OA) observed over Look Rock, Tennessee (a SAS measurement site about 500 miles to

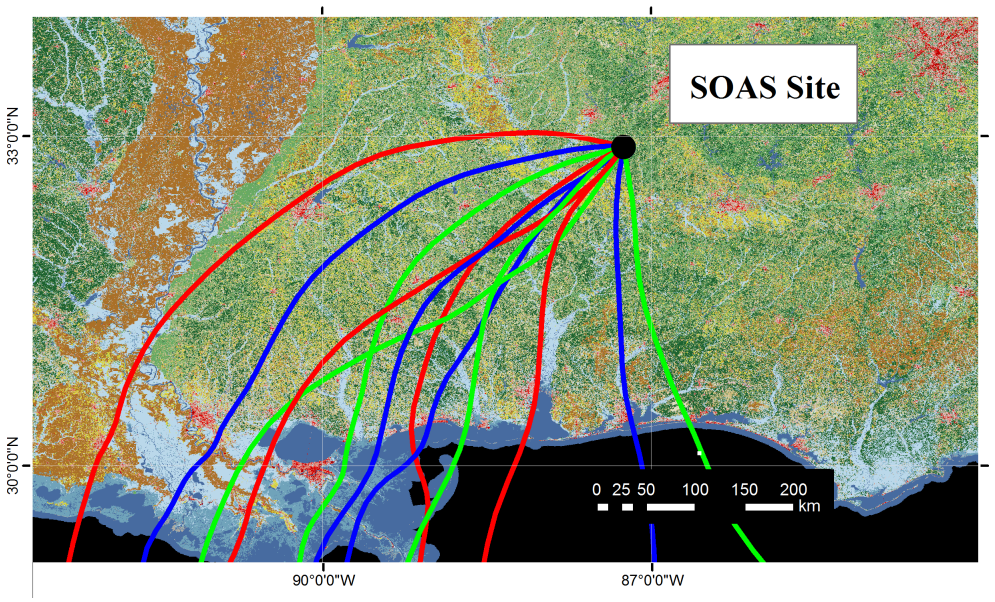

FIGURE 2.9: Backward trajectories of air masses from the SOAS site going back 48 hours using the NOAA Hysplit Trajectory Model at 100m height using the National Centers for Environmental Prediction (NCEP) Global Data Assimilation System half degree model. The trajectories start every 4 hours and are superimposed on land use data from the National Land Cover Database 2011. The dark green colours denote areas covered by deciduous forests, while lighter green colours denote areas covered by mixed forests, with similar characteristics to the forest at the SOAS site.

the north-north-east of Centerville, Alabama) to the MO-OOA observed at the Centerville site showing that MO-OOA has a strong regional signal and we consequently assume that MO-OOA is being transported from the south. Moreover, BBOA only increased at the SOAS site during smoke plume events, which are associated with an increase in levels of measured levoglucosan (Washenfelder et al., 2015). Based on this, we assume that MO-OOA and BBOA are non-local SOA for the domains of the mixed-layer model and are therefore not part of the observations that are used to constrain the model.

2.7 Sensitivity analysis on dynamic and chemistry processes

In order to test the sensitivity of the modelled SOA concentration to surface and dynamical factors, we perform a set of additional experiments to test the sensitivity of SOA concentrations to deposition of ISOPOOH and IEPOX, the FT-concentrations of ISOPOOH-SOA and IEPOX-SOA, the ventilation flux and advection of SOA.

Figure 2.10a shows that dry deposition of ISOPOOH and IEPOX decreases the SOA concentration in the mixed layer: As deposition removes isoprene-SOA precursors from the ABL, it will also reduce the mixing ratio of SOA in the ABL. The prescribed deposition velocities of ISOPOOH and IEPOX are considerable, compared to the deposition velocity of SOA (3 cm/s

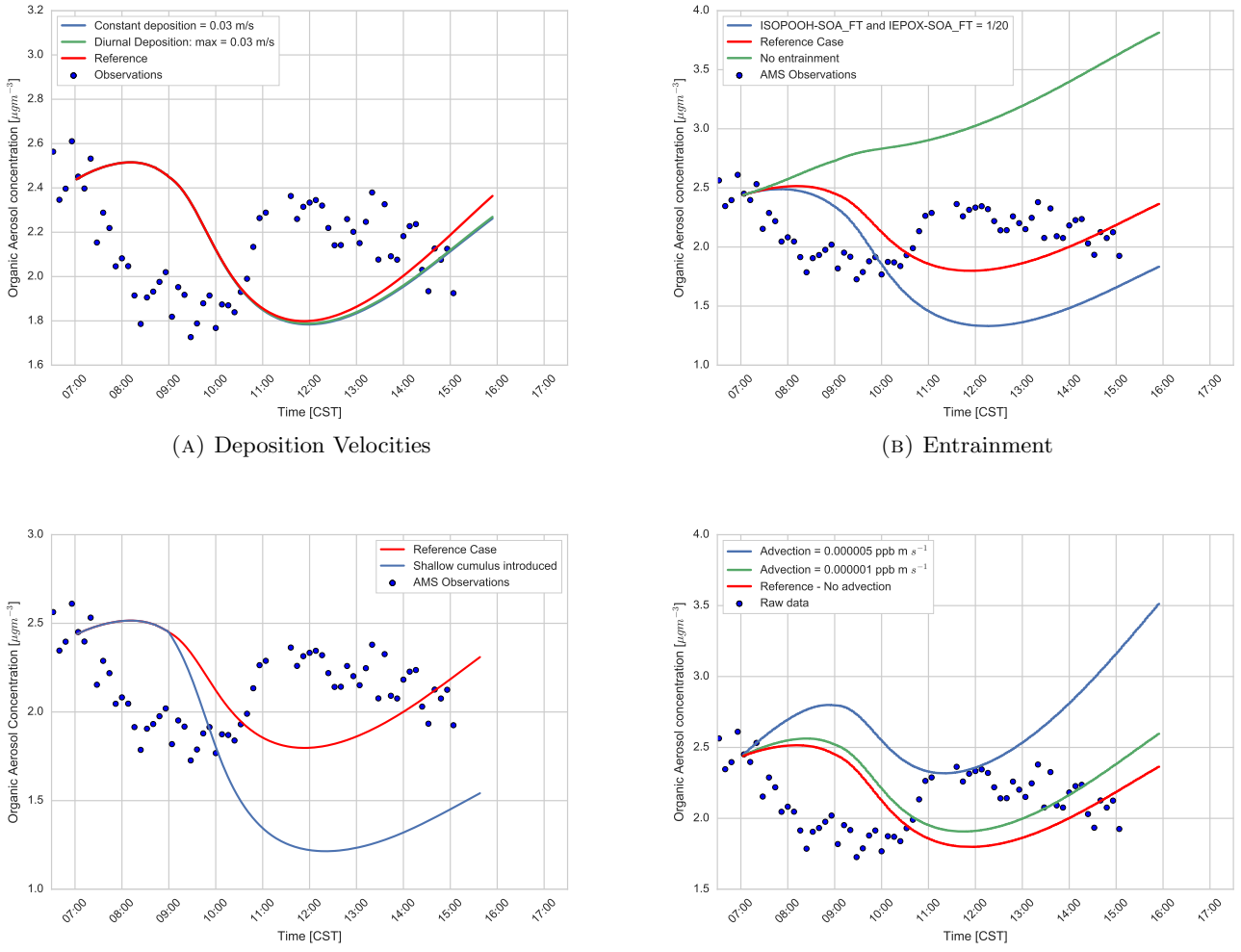

(A) Deposition Velocities

(B) Entrainment

(C) Ventilation

(D) Advection

FIGURE 2.10: Effect of (a) ISOPOOH and IEPOX deposition, (b) FT concentrations of the SOA composites, (c) ventilation due to mass flux and (d) advection of SOA on the diurnal evolution of SOA.

for ISOPOOH and IEPOX (Nguyen et al., 2015b) compared to 0.02 cm/s for aerosol mass (Farmer et al., 2013)). The deposition causes the total SOA concentration to decrease at the end of the experiment though the root mean squared error (RMSE) is slightly higher for the experiments with the deposition turned on compared with the reference case. The RMSE for constant deposition velocity from observations is 2.2% higher (RMSE = 0.437 μgm^{-3}) than the reference case (RMSE = 0.433 μgm^{-3}), while the RMSE for the diurnal deposition velocity is 1.8% higher (RMSE = 0.435 μgm^{-3}). However, the RMSE is higher as deposition lowers the SOA concentration from 12:00 CST, while the observed SOA is still increasing. The difference from the reference case at the end of the experiment is 0.1 μgm^{-3}, and there is almost no discernible difference observed when a diurnal cycle in the deposition velocity is applied, compared to a constant deposition velocity. As the observed SOA concentrations are lower at the end of the simulation, this brings the model closer to the observations at the end of the

experiment. Dry deposition acts as a loss to the mixing ratio of IEPOX and ISOPOOH in the BL that is missed when only the chemical destruction is taken into account (Karl et al., 2009). Nguyen et al. (2015b) report that dry deposition is a dominant diurnal sink for small-saturated oxygenates (including IEPOX and ISOPOOH), while Bessagnet et al. (2010) estimate a 50% overestimation of SOA concentrations if dry deposition of SVOCs is omitted, although this is open to much debate. Dry deposition accounts for approximately 45% of IEPOX loss (Bates et al., 2014) as reactive uptake into the aerosol phase is slow (Gaston et al., 2014; Krechmer et al., 2015), though IEPOX loss through dry deposition is reduced in the presence of acidic sulphate particles (Nguyen et al., 2015b). Hence, an inclusion of this loss term will have an effect on the modelled diurnal evolution of SOA. This is especially important because the SOA concentration is overestimated at the end of the day, implying a lack of loss terms in the model. The SOA concentration at 15:00 CST is better represented when dry deposition is included.

SOA concentrations are much lower in the reference case than in the case where uniform SOA concentrations are prescribed in ABL and FT (Figure 2.10b), which shows the effect of entrainment on the SOA concentrations in the ABL. When uniform concentrations for the organics in the BL and the FT are used, it can be seen that the total SOA concentration reaches approximately 3.6 μgm^{-3} by the end of the simulation (much higher than the observed at 2.0 μgm^{-3}). This rise is due to the production of SOA during the day through chemical reactions. Using the FT concentration of the total SOA observed in the SENEX flight (which is the control case), we found that the diurnal evolution of SOA decreases considerably to 2.3 μgm^{-3} at the end of the simulation. The RMSE for the case with no entrainment is 0.9 μgm^{-3} compared to the RMSE of the reference case, which is 0.43 μgm^{-3}. This decrease is due to dilution of SOA in the BL due to entrainment, which is less pronounced when the FT has the same SOA concentration as the BL. This difference is seen in Janssen et al. (2012), who discussed the importance of background OA concentration in the FT; if there was a large jump of background OA between the BL and FT it had a significant effect on diurnal SOA evolution. Mixing ratios and concentrations are generally lower in the FT compared to the BL (which is seen in the case of SOA in Figure 2.2), and hence entrainment dilutes the mixing ratios and concentrations in the BL (Karl et al., 2007, 2009). Hence, it is important to consider the profiles of IEPOX-SOA and ISOPOOH-SOA, and if there is a large jump between the BL and FT for these species, there will be an impact on the BL evolution of SOA. Vertical profiles of IEPOX-SOA show a large jump of IEPOX-SOA atop the BL in southeasternern US in 2009 (Froyd et al., 2010). Therefore, we prescribe FT concentrations of ISOPOOH-SOA and IEPOX-SOA at 5% of the mixed layer concentrations in a third experiment. This reduces the mixed layer concentration of SOA at the end of the day even more than in the reference case (to 1.7 μgm^{-3}). The RMSE of the simulation with observations increases to 0.66 μgm^{-3}, indicating that the jump of concentrations at the top of

the BL might be too big. However, SOA concentrations in the summer decay with altitude and the total SOA concentration decreases by about 90% from BL to FT; so the prescribed FT concentrations of ISOPOOH-SOA and IEPOX-SOA seem reasonable (Wagner et al., 2015).

Figure 2.10c shows that the presence of shallow cumulus clouds and the associated effect of ventilation due to mass flux reduces SOA concentration (by 0.8 μgm^{-3} compared to the reference case at the end of the simulation) in the mixed layer due to upward transport. It is important to note that in the presence of these fair weather clouds, the mixed layer is essentially the sub-cloud layer; the clouds are formed depending on heat and moisture in the BL and since the relative humidity at the BL top is less than 100% only strong updrafts can reach a level of condensation to form these non-uniform cloud patches (van Stratum et al., 2014). The mass flux associated with these clouds dampens the BL growth (Stull, 1988) and also causes the ventilation flux of scalars. The decrease in SOA concentration is most profound after 09:00 CST, two hours after the simulation starts. This is because the shallow cumulus module, and the hence ventilation of SOA due to mass flux, only starts at 09:00 CST and due to the ventilation effect the SOA concentration in the mixed layer decreases from 2.4μgm^{-3} to 1.2 μgm^{-3} in a matter of 3 hours. This difference is much higher compared to the case with dry deposition. However, the difference between the reference case and the case with no entrainment is higher than that between the reference case and the ventilation case at the end of the simulation (higher by 0.4 μgm^{-3}), hence entrainment has a larger effect than ventilation. The RMSE of the experiment is 0.7 μgm^{-3}, which is quite high, but as the day of the observations was not cloudy this sensitivity analysis is not expected to actually capture the observations. SOA and SOA precursors are both transported from the sub-cloud layer to the cloud layer and, consequently, the mixed layer concentration decreases, which has been studied extensively with large eddy simulations (van Stratum et al., 2014; Ouwersloot et al., 2013). The occurrence of clouds should also diminish radiation that reaches the boundary layer and the photochemical reactions in the BL would be affected by the interruption of radiation, which would further decrease aerosol formation (Vilà-Guerau de Arellano et al., 2015). Moreover, the surface heat fluxes are reduced with a decrease in incoming radiation, though this has a negative feedback on cloud formation (Feingold et al., 2005). A decrease in aerosol can (depending on the size distribution of aerosols), however, have an impact on cloud properties, as cloud formation is affected by CCN size and availability (Novakov and Penner, 1993), which is a fraction of the aerosol population. Hence, on a longer time scale, the drop in aerosol could alter cloud properties, which could eventually have a positive effect on the aerosol concentration in the BL.

Lastly, in order to study the effect of advection of SOA, which we discussed in Section 2.6 and observed in Figure 2.9, we found that that introducing advection of SOA has a positive effect on SOA concentrations in the mixed layer (See Figure 2.10d). Not including advection

of SOA assumes horizontal homogeneity for SOA concentration in the area, and as SOA tends to be long-lived, SOA advection likely has a contribution to local SOA budget (Janssen et al., 2013). In the previous section, we concluded that a substantial amount of SOA (in the form of MO-OOA and BBOA) arrived at the SOAS measurement site by advection. Though we have classified it as non-local it is interesting to study the influence it can have on the OA produced in the system, especially as SOA formation depends on older SOA that is present in the system. Figure 2.10d shows that in case of a slight increase in advection of SOA by $5 \cdot 10^{-6}$ ppb m/s the SOA concentration in the mixed layer increases quite markedly (up to 3.4 μgm^{-3}), as advection increases the amount of SOA entering the BL. The RMSE of this experiment is 0.63 μgm^{-3}. In the case that advection is set to $1 \cdot 10^{-6}$ ppb m/s the RMSE compared to the reference case is 2.3% better at capturing the observations. An increase of SOA concentration in the BL also has a positive feedback of SOA formed in the system, as an increase in aerosol surface leads to more efficient SOA formation (Donahue et al., 2006; Janssen et al., 2012). Here we have used a constant advection of SOA with time. However, as seen in the observations Figure 2.1, MO-OOA is not advected at the same rate at all times, thus indicating a diurnal variability. Moreover, the peak of observed SOA concentration between 11:00 CST and 12:00 CST is somewhat captured by the model when advection is $5 \cdot 10^{-6}$ ppb m/s. The SOA in southeastern US is considered to have a regional signal and is prone to regional transport (Lin et al., 2013; Xu et al., 2015b), hence advection needs to be taken into account when modelling SOA.

Three of the aforementioned sensitivity analyses concern factors that could be altered in the reference case to better capture the observations; dry deposition forms a loss term that reduces the mixing ratio of SOA precursors in the mixed layer, FT concentrations alter the dilution brought about by entrainment in the boundary layer and advection can increase the SOA concentrations in the BL both directly and indirectly. Lastly, a case study on the presence of clouds, which are characteristically found in the SOAS measurement site in the summer months, shows the loss of SOA to the cloud layer. Through these sensitivity analyses we find that diurnal evolution of SOA is also sensitive to, besides SOA formation, dynamical and surface factors, and hence needs to be studied in such an integrated approach. Data collection also needs to take into account factors like FT concentration or mixing ratios and dry deposition, which could be used to constrain this model better. Moreover, factors like advection need to be better resolved and taken into account in the model. Through these sensitivity analyses, we have modelled the all the main processes described by Equation (2.4) that have an effect on the SOA diurnal evolution. Hereafter, we analyse the contribution of the different processes on the SOA tendency.

2.8 VOC, SVOC and SOA Budgets

Figure 2.12 shows budgets of three species: isoprene, a CiI species (which is an isoprene related SVOC, called C1I) and OA, based on the equations (Equation (2.21) to Equation (2.25)) in Section 2.4. In these equations the BL height modulates the emission, deposition and entrainment terms (which is also driven by the entrainment velocity), thereby connecting the chemical evolution in the BL to dynamics of the BL (Janssen et al., 2013).

The isoprene budget is largely driven by isoprene emission and chemical loss and in smaller amounts, by entrainment. The isoprene emission tendency peaks at around 10:00 CST, while the isoprene flux (see figure Figure 2.6), peaks at 12:00 CST. This dephase is due to the BL height growth, since the emission tendency depends on the BL height evolution. A similar difference in timing is also seen in Su et al. (2016). The difference in the emission diurnal evolution compared to Su et al. (2016), however, shows that emission tendency peaks much earlier in Su et al. (2016), where the emission fluxes are prescribed. Isoprene chemical loss is driven by the isoprene reaction with OH to form isoprene peroxy radicals (IRO2), which subsequently lead to isoprene SOA formation. This chemical loss is largest at 09:30 CST. The entrainment tendency of isoprene serves as a loss term, since it acts to dilute the isoprene concentration. The initial contribution of this term is 0 and rises to around 12% at 10:00 CST after which it falls to almost 0 again by 16:00 CST. The total tendency of isoprene is relatively flat as the chemical loss, entrainment and emission terms modulate the total tendency. The emission tendency has a contribution of 70% at the start of the simulation to 50% at the end, while chemistry contribution is around 30% at the start and 50% at the end. The total tendency stays positive, because the emission tendency's contribution is larger than those of chemical loss and entrainment, although it decreases to 0 after 14:00 CST, which is reflected in the mixing ratio of isoprene, which is constant after 14:00 CST (See Figure 2.7a). Unlike in Janssen et al. (2013) and Vilà-Guerau de Arellano et al. (2009) the total isoprene tendency here does not decrease below 0. In our budget, the chemistry always contributes more to the isoprene budget than entrainment, while in Janssen et al. (2013) there is a larger entrainment tendency contribution in the late morning, which is probably higher as the entrainment velocity is higher (13 cm/s versus 8.33 cm/s here). The budget in Vilà-Guerau de Arellano et al. (2009) dips below 0 in the afternoon, as the chemistry contribution, which is almost always higher than entrainment, is higher than emission in the afternoon, which does not happen in our case.

The largest contribution to the C1I budget is formed by the chemical production term (Figure 2.12b). The C1I chemistry peaks around 09:15 CST, while the total C1I tendency peaks around 08:45 CST. The initial contribution of chemistry to the total tendency is 100%, which

decreases to 60% by 10:00 CST, and stays there until the end of the simulation. The contribution of entrainment rises from 0 at 07:00 CST to 35% at 10:00 CST after which it gradually falls to 0 at 16:00 CST. The contribution of deposition rises from 0 at the start to 40% by the end of the simulation. The entrainment term is a larger loss term than deposition, especially between 09:00 and 14:00 CST, and peaks at 10:00 CST (as entrainment velocity is at its peak at 8.33 cm/s). The deposition term (with a constant V_d = 2.4 cm/s) is highest around 09:00 CST, after which it decreases slightly until the end of the simulation, although at the end it still has a large contribution. The C1I chemical formation term peaks around the same time as the chemical loss of isoprene, because the C1I production depends on IRO2 formation, which peaks with isoprene loss. The production of C1I is about a factor 10^3 smaller than the isoprene loss, which is due to the low yield of C1I (0.001), which is consistent with Janssen et al. (2013) (it is important to note that this is just one of the CiI species, the others have higher yields). The C1I budget is similar to Janssen et al. (2013); though entrainment was a larger factor in Borneo. CiI is formed here only through the high-NO_x pathway, and after one more intermediate step in the gas-phase, compared to in Janssen et al. (2013). Hence, despite a higher isoprene chemical destruction than at Borneo, we get about the same production of C1I as Janssen et al. (2013).

The SOA budget shows a strong dependency on the entrainment of background OA (OA_{BG}). The contribution of OA_{BG} in the early morning is large, however, the ratio of the factors that make up the OA_{BG} in the FT are not known. This makes it difficult to allocate how much of the OA_{BG} is made of aged isoprene SOA and monoterpene SOA, that either persists locally or was advected, and how much is formed during the night or daytime. The decrease observed in the total SOA budget around 9:00 CST is caused by the OA_{BG} entrainment, and since the production terms are low at this time the SOA budget is largely driven by entrainment. The contribution of OA_{BG} to SOA tendency is substantial, rising sharply from 0 at 07:10 CST to almost 95% at 09:30 after which it falls to 3% by the end of the simulation. This is consistent with Janssen et al. (2012) who found that the OA_{BG} entrainment has a sizable contribution to the SOA budget if there is a strong jump between BL and FT and were able to study the role of the OA_{BG} that persists in the residual layer. The residual layer, that decouples from the nocturnal boundary layer, can act as a reservoir of SOA in the early hours of the morning and thereby has an effect on the entrainment flux and SOA evolution in the BL (Li et al., 2014). The OA_{BG} concentration has an effect on the SOA formed through the VBS module; the fresh aerosol formed through G/P-partitioning depends on the amount of pre-existing aerosol in the system (Janssen et al., 2012). The OA_{BG} entrainment dilutes the concentration of SOA in the BL, which consequently makes the G/P partitioning less efficient and leads to less SOA formation. As discussed in Section 2.7, the effect of dilution can be seen when we compare the case where OA_{BG} concentrations are uniform in the BL and FT compared to the reference case,

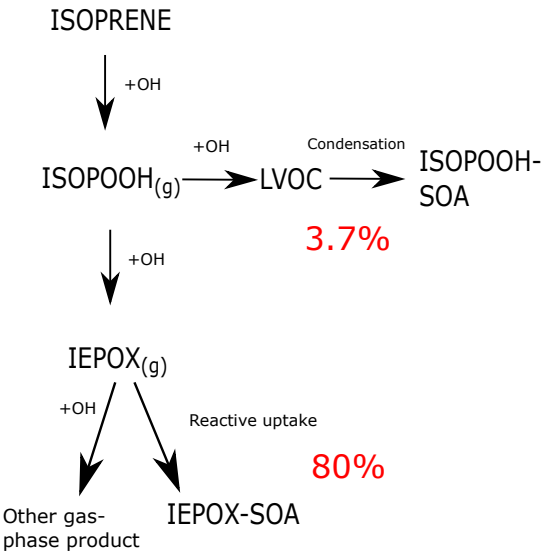

FIGURE 2.11: The oxidation products of Isoprene, with g denoting gases, from Figure 2.4. The percentage in red signifies the contribution of the isoprene SOA factor on the total SOA budget at the end of the day (16:00 CST).

and the effect of dilution is rather large (See Figure 2.10b, where no entrainment has uniform OA_{BG} concentrations, while the reference case is based on observations).

The contribution of SOA formation by chemical reactions to the SOA budget is less marked than entrainment. The chemistry tendency is split up between monoterpene SOA (TSOA), isoprene SOA (ISOA), which is further divided into ISOA through G/P partitioning (VBS-ISOA), ISOPOOH-SOA and IEPOX-SOA. The TSOA has a large contribution in the early morning (90%), but it falls rapidly to 0 at 09:30 CST. At the end of the simulation, the TSOA contribution rises to 9%. The VBS-ISOA contribution is quite small, at 8% between 07:00 CST and 09:00 CST to 1% at 10:00 CST. It rises slightly in the afternoon (peaking at 4%), though by 16:00 CST the contribution is only 2%. As the OA_{BG} entrainment falls, SOA concentration increases (after 12:00 CST), and is taken over by SOA formation through reactive uptake (IEPOX-SOA). The IEPOX-SOA contribution rises steadily from 0 at 07:00 CST to almost 80% at the end of the simulation. Formation of ISOPOOH-SOA has a minor effect on the total OA budget. The contribution of ISOPOOH-SOA is 0 at 07:00 CST, and it rises slightly with a peak of around 3.7% at 15:00 CST. The contribution at the end of the day for isoprene SOA can be visualised in Figure 2.11.

In the morning, TSOA has the highest contribution to SOA formation, while after 10:00 CST ISOA has a larger contribution to SOA formation, especially IEPOX-SOA. The TSOA contribution dominated the night-time SOA concentration and consequently, the early morning SOA, as monoterpene derived SOA makes up the bulk of LO-OOA, which peaks at night-time (Ayres et al., 2015). ISOA, on the other hand, is known to contribute mostly during the daytime (Ayres et al., 2015), as reflected in the budget. The total TSOA is negative after 09:00 CST, and if

we analyse at the C1T tendency of TSOA (Figure 15), the total C1T tendency also becomes negative. This is due to the entrainment of C1T, and causes the TSOA tendency to become negative between 09:30 and 12:00 CST. It is important to note that the decrease in total SOA tendency in the morning is seen in Figure 2.7 the rapid drop of SOA concentration seen in the model in the morning.

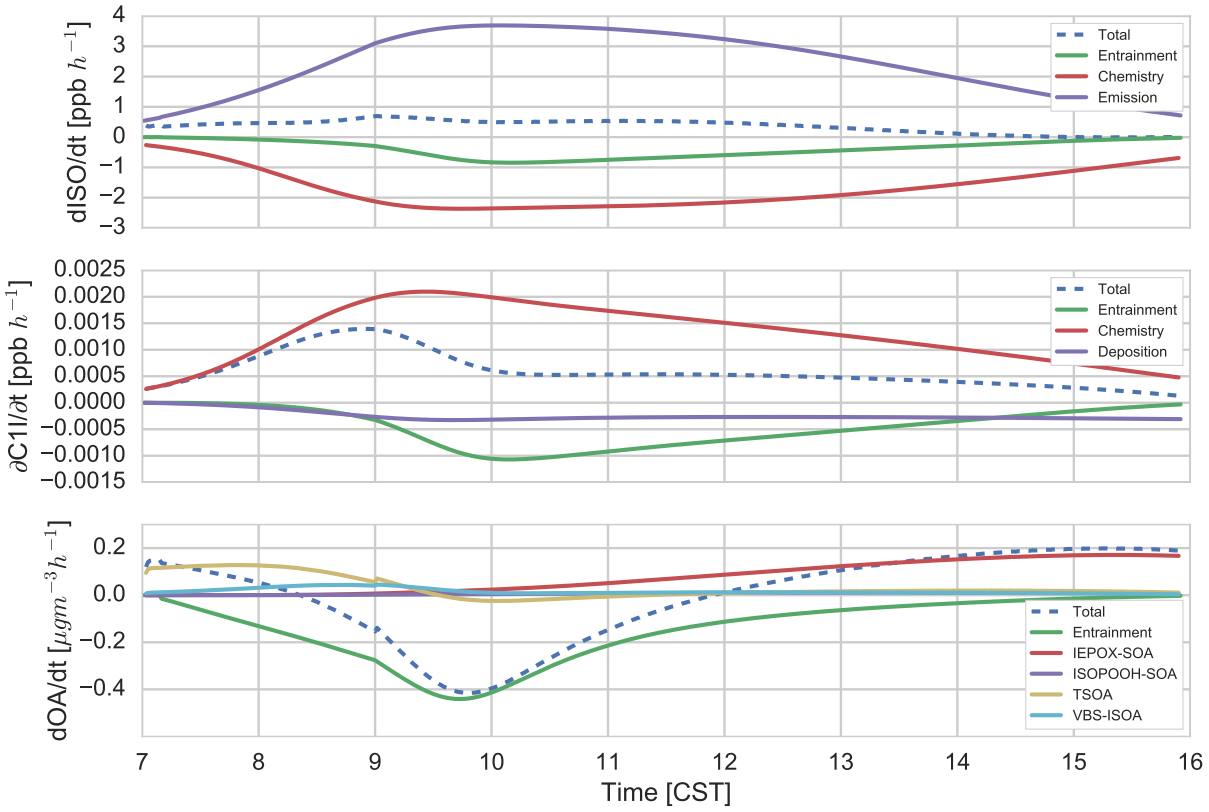

FIGURE 2.12: The isoprene (top), an isoprene-derived semi-volatile organic compound (C1I) (mid) and the total SOA (bottom) budget. They are divided in total tendency (dashed), contribution due to entrainment (green), contribution due to chemistry for isoprene and C1I (red) and deposition/emission contribution (purple). For total OA the chemistry contribution is split into IEPOX-SOA (red), ISOPOOH-SOA (purple), monoterpene-derived SOA (yellow) and gas/partitioning isoprene SOA, called VBS-ISOA (cyan).

Conclusion

We study and quantify the dynamics, gas-phase chemistry and SOA concentrations above the Southern Oxidant and Aerosol Study (SOAS) campaign site. We then model the SOA concentration at the SOAS measurement site in southeastern US, using a mixed-layer chemistry model (MXLCH). To this end, MXLCH was updated to include new isoprene-SOA formation pathways that are significant for this region. The numerical experiments were coupled to the surface in order to interactively calculate the surface heat fluxes and the emissions of isoprene and monoterpenes. We distinguish between locally-produced SOA and non-locally produced SOA and a series of numerical experiments and SOA budget analysis were carried out.

The gas-phase chemistry and diurnal dynamics were previously succesfully modelled using the MXLCH model. In this study, we were able to incorporate and represent the interactively surface heat fluxes successfully compared to the observations, which peaked at or just before noon, though the sensible heat flux is on the high end of the observations (peak of 0.13 K m^{-1}). The monoterpene emissions were captured well for most of the modelling period, though overestimated in the last hour of the simulation (by 0.01 ppb m s^{-1}), whereas the isoprene emissions were underestimated compared to the observations (by approximately 0.2 ppb m s^{-1}), though we were able to successfully capture the mixing ratio of isoprene. Our reference case was not able to capture the diurnal evolution of SOA that was observed at the SOAS measurement site very well, with an overestimation in the model at the end of the simulation. Moreover, there was an overestimation of SOA concentrations in the morning and an underestimation in the afternoon, the model seems to be in an anti-phase with the observations. For the individual SOA components, we find that ISOPOOH-SOA evolution is well represented, whereas the IEPOX-SOA diurnal evolution is not captured that well by the model. A potential improvement not accounted for in our study is the pH dependence of IEPOX-SOA and coupling the daily evolution of IEPOX-SOA to the sulphate diurnal evolution. However, we argue that the inability of the model to represent the LO-OOA (which is mostly monoterpene-derived) evolution causes the largest uncertainty between the modelled and the observed diurnal evolution of SOA. We did not change the monoterpene aerosol mechanism compared to previous studies; loss terms for monoterpene SOA (especially those that are dominant in the morning), advection of SOA, and

early morning FT profiles of LO-OOA (to account for LO-OOA in the residual layer) need to be studied, measured and modelled. The influence of monoterpenes will be addressed in future studies.

In order to apportion SOA into locally and non-locally produced SOA, we analysed air mass trajectories that arriving at the measurement site. Air masses arrived predominantly form the South and since their trajectories crossed tracts of forested area, the more-aged SOA could be picked up from these forests. The BBOA and MO-OOA factors are considered a regional footprint, which then could have been picked up and processed in by the air masses at the SOAS site.

A series of numerical experiments were carried out to evaluate the sensitivity of the model to different surface and dynamic variables, with the aim of determining which factors could improve the model. Focusing first on the upper conditions, we use the FT observations of SOA, and the model was able to account for entrainment in a more realistic way and consequently the modelled SOA concentrations are closer to the observations. Turning our focus on surface effects, we used the enhanced dry deposition of ISOPOOH and IEPOX which helped in lowering the overestimation of the SOA concentration at the end of the day. In order to take into account long-rage transport, we analyse which advection of SOA increases the SOA concentration in the model, which might help in capturing part of the increase in observed SOA concentration in the afternoon, though it makes the discrepancy between the model and observations in the morning larger. In our separation of SOA into local and non-local SOA we assume that all MO-OOA is being advected; MO-OOA could also result from extremely fast oxidation and could then be locally produced. This further complicates the model-measurement comparison. To study a top of the BL effect we introduce a ventilation flux, which, in the presence of shallow cumulus clouds, transports SOA from the sub-cloud layer to the cloud layer due to associated mass flux, thereby reducing the SOA concentration in the BL; the representative day is sunny hence the case study is not expected to improve the model. Therefore, we need to have good FT observations of SOA (especially early morning), dry deposition measurements of precursors and account for advection of SOA. From these analyses we can see that the SOA diurnal evolution is sensitive to dynamic, surface and chemical factors, and in order to improve the model we need an integrated approach to address all these factors.

Lastly, from the budget calculations, it is apparent that the SOA diurnal evolution is influenced by contributions from dynamical processes (with entrainment having the largest contribution on total SOA tendency), surface conditions (which dominate the VOC tendency) and chemistry (which dominates the intermediate SVOC tendency). The budget analysis also shows that during the day isoprene-derived SOA has a high contribution to total SOA concentration, while in the early hours of the day monoterpene-derived SOA has a larger contribution. We conclude

that the modelling of the diurnal evolution of SOA improved with advances in understanding the chemical mechanisms behind it, although there is room for improvement.

2.9 Acknowledgements

Data for the gas-phase chemistry and dynamics from the SAS studies was provided by Luping Su, while the AMS SOA observations and PMF factorization product data were provided by Weiwei Hu and Juliane Fry. Insight regarding the implementation of the MEGAN model was provided by Alex Guenther. Jose-Luis Jimenez provided information on the new aerosol mechanisms.

Dynamical Set Up

TABLE 3: Dynamics: Initial and boundary layer conditions to reproduce the dynamical properties of June 11, 2013 from the SOAS measurement campaign, based on Su et al. (2016).

Property	Value	Units
Initial boundary layer height (h)	500	m
Flow divergence factor for subsidence (w_{sls})	$9 \cdot 10^{-6}$	s^{-1}
Surface sensible heat flux ($(\overline{w'\theta'})_s$)	0.10	K m s^{-1}
Entrainment ratio (β)	0.2	[-]
Initial mixed layer potential temperature ($\langle\theta\rangle$)	296.6	K
Potential temperature lapse rate (γ_θ)	0.001	K m^{-1}
Initial potential temperature jump ($\Delta\theta$)	1.5	K
Advection of potential temperature A_θ	$6.4 \cdot 10^{-4}$	K s^{-1}
Surface moisture flux ($(\overline{w'q'})_s$)	0.15	g kg^{-1} m s^{-1}
Initial mixed layer specific moisture ($\langle q\rangle$)	16.8	g kg^{-1}
Specific moisture lapse rate (γ_q)	-0.004	g kg^{-1} m^{-1}
Initial specific moisture jump (Δq)	-2.5	g kg^{-1}
Advection of specific moisture (A_q)	$1.5 \cdot 10^{-4}$	g kg^{-1} s^{-1}
Pressure	1005.1	Pa

.1 Ventilation Calculation

The following equations, based on van Stratum et al. (2014) determine the ventilation effect due to clouds on all scalars, though we only study the effect on SOA.

Equation (26) shows the scalar budget in the mixed layer (excluding the advection term).

$$\frac{\partial\langle C\rangle}{\partial t} = \frac{(\overline{w'C'})_s - (\overline{w'C'})_e - (\overline{w'C'})_M}{h} + S_c \tag{26}$$

Here $\langle C\rangle$ is the bulk scalar concentration in the ABL in ppb, while $(\overline{w'C'})_s$ and $(\overline{w'C'})_e$ are the vertical chemical fluxes at the surface, at the entrainment zone (entrainment flux) and $(\overline{w'C'})_M$ the mass flux of the scalar due to presence of clouds (all in ppb m s^{-1}).

This equation can be rewritten to include the representation of entrainment and the mass flux transport in Equation (27). The budget equation then reads:

$$\frac{\partial\langle C\rangle}{\partial t} = \frac{(\overline{w'C'})_s + w_e\Delta_c - M_{\sigma c}|_h}{h} + S_c \tag{27}$$

w_e is the entrainment velocity (m s^{-1}), Δ_c is the jump of the scalar in ppb between the ABL and the FT. The mass flux of the scalar ($M_{\sigma c}|_h$) is be calculated by the variance of the scalar at the top of the ABL ($\sigma_c|_h$) and the vertical M, which is the mass flux (in m s^{-1}), as seen in Equation (28).

$$M_{\sigma c}|_h = \sqrt{\sigma_c|_h} \cdot M \tag{28}$$

where

$$\sigma_c|_h = -(\overline{w'C'})_s + (\overline{w'C'})_M \cdot \frac{\Delta c}{\Delta z}\frac{h}{w_*} \tag{29}$$

The variance ($\sigma_c|_h$) is calculated by the surface vertical scalar flux and the mass flux of the scalar multiplied by the scalar jump between BL and FT and Δz is the depth of the transition layer. w_c is closely related to the convective velocity scale, w_* ($w_c \approx w_*$), which is calculated by Equation (30). A positively buoyant layer develops above the mixed layer due to clouds so we use the scaling as per (Horn et al., 2015).

$$w_* = \left(\frac{g}{\theta_{vo}}(\overline{w'\theta'_v})_s h)\right)^{\frac{1}{3}} \tag{30}$$

In the aforementioned equation, g is the gravitational acceleration (in m s^{-2}), θ_{vo} is the reference virtual potential temperature (in K) in the sub-cloud layer (which is equal to $\langle\theta_v\rangle$, the mixed layer virtual potential temperature), $(\overline{w'\theta'_v})_s$ is the virtual potential temperature flux (K m s^{-1}) at the surface and h is the boundary layer height.

The mass flux, M, is related to cloud core fraction, saturation and specific humidity and calculated as per van Stratum et al. (2014)

Chemical Set Up

TABLE 4: Initial mixing ratio in the boundary layer and FT surface emission/deposition fluxes of reactants based on Su et al. (2016). Gas-phase chemistry conditions are based on ground observations at SEARCH site, flux tower observations at the AABC tower and aircraft observations (WASP system and NCAR-130 flight) and then averaged for 5, 6, 8, 10-13 June (Su et al., 2016). Observations for secondary organic aerosol are from the Aerosol Mass Spectrometer on the SEARCH ground site and a SENEX flight on 11 June. Species with 0 initial concentrations and emissions are not included in the table.

Species	Initial mixing ratio (ppb)		Surface emission/deposition
	BL mixing ratio	FT mixing ratio	(ppb m s^{-1})
O_3	12.9	51	2.3*
NO	0.1	0.05	$-0.005\sin(\frac{\pi t}{t_d})$
NO_2	0.8	0.06	$0.005\sin(\frac{\pi t}{t_d})$
HCHO	1.0	1.1	0.0
ISO	0.6	0.0	**
MVK+MACR	0.6	0.6	2.4*
TERP	1.1	0.0	**
OA_{BG}	0.32	0.15	0.0
CiI	0.0	0.0	2.4*
CiT	0.0	0.0	2.4*
ISOPOOH	0.0	0.0	0.0***
IEPOX	0.0	0.0	0.0***
IEPOX-SOA	0.06	0.06	0.0
ISOPOOH-SOA	0.014	0.014	0.0

* Dry deposition velocity in cm s^{-1}

**Interactively calculated by MEGAN (Section 2.2.3)

***Dry deposition velocity used in sensitivity analysis (3 or $3\sin(\frac{\pi t}{t_d})$ cm s^{-1})

TABLE 5: Chemical Reaction Scheme. In the reaction rates, T is the absolute temperature in Kelvin and is the solar zenith angle. First-order reaction rates are in s^{-1}, second-order reaction rates in $cm^3 molecule^1 s^1$. $\alpha_1^I - \alpha_4^I$ and $\alpha_1^T - \alpha_4^T$are the stoichiometric coefficients for ISO and TERP, respectively. PRODUCTS are the species which are not further evaluated in this chemical reaction scheme. Reaction of isoprene with O_3 is not considered (Janssen et al., 2013; Su et al., 2016) and new reactions adapted from Hu et al. (2016).

Number	Reaction	Reaction Rate
R1	$O_3 + h\nu \rightarrow O^1D + O_2$	$3.00 \cdot 10^{-5} \cdot e^{\frac{-0.575}{\cos(\chi)}}$
R2	$O^1D + H_2O \rightarrow 2OH$	$1.63 \cdot 10^{-10} \cdot e^{\frac{60}{T}}$
R3	$O^1D + N_2 \rightarrow O_3$	$2.15 \cdot 10^{-11} \cdot e^{\frac{110}{T}}$
R4	$O^1D + O_2 \rightarrow O_3$	$3.30 \cdot 10^{-11} \cdot e^{\frac{55}{T}}$
R5	$NO_2 + h\nu \rightarrow NO + O_3$	$1.67 \cdot 10^{-2} e^{\frac{-0.575}{\cos(\chi)}}$
R6	$CH_2O + h\nu \rightarrow HO_2$	$1.47 \cdot 10^{-4} \cdot e^{\frac{-0.575}{\cos(\chi)}}$
R7	$OH + CO \rightarrow HO_2$	$2.40 \cdot 10^{-13}$
R8	$OH + CH_4 \rightarrow CH_3O_2$	$2.45 \cdot 10^{-12} \cdot e^{\frac{-1775}{T}}$
R9	$OH + ISO \rightarrow IRO_2$	$2.70 \cdot 10^{-11} \cdot exp\frac{390}{T}$
R10	$OH + [MVK+MACR] \rightarrow HO_2 + CH_2O$	$2.40 \cdot 10^{-11}$
R11	$OH + HO_2 \rightarrow H_2O + O_2$	$4.80 \cdot 10^{-11} \cdot e^{\frac{250}{T}}$
R12	$OH + H_2O_2 \rightarrow H_2O + HO_2$	$2.90 \cdot 10^{-12} \cdot e^{\frac{-160}{T}}$
R13	$HO_2 + O_3 \rightarrow OH + 2O_2$	$2.03 \cdot 10^{-16} \cdot (\frac{T}{300})^{4.57} \cdot e^{\frac{693}{T}}$
R14	$HO_2 + NO \rightarrow OH + NO_2$	$3.50 \cdot 10^{-12} \cdot e^{\frac{250}{T}}$
R15	$CH_3O_2 + NO \rightarrow HO_2 + NO_2 + CH_2O$	$2.80 \cdot 10^{-12} \cdot e^{\frac{300}{T}}$
R16	$IRO_2 + NO \rightarrow HO_2 + NO_2 + CH_2O + 0.7[MVK+MACR] + \alpha_1^I IC_1 + \alpha_2^I IC_2 + \alpha_3^I IC_3$	$1.00 \cdot 10^{-11}$
R17	$OH + CH_2O \rightarrow HO_2$	$5.50 \cdot 10^{-12} \cdot e^{\frac{125}{T}}$
R18	$2HO_2 \rightarrow H_2O_2 + O_2$	*
R19	$IRO_2 + HO_2 \rightarrow 0.12OH + 0.88ISOPOOH + 0.12HO_2 + 0.073MVK + PRODUC$	$7.40 \cdot 10^{-13} \cdot exp\frac{390}{T}$
R20	$CH_3O_2 + HO_2 = PRODUC$	$4.10 \cdot 10^{-13} \cdot e^{\frac{750}{T}}$
R21	$OH + NO_2 \rightarrow HNO_3$	$3.50 \cdot 10^{-12} \cdot e^{\frac{340}{T}}$
R22	$NO + O_3 \rightarrow NO_2 + O_2$	$3.00 \cdot 10^{-12} \cdot e^{\frac{-1500}{T}}$
R23	$NO + NO_3 \rightarrow 2NO_2$	$1.80 \cdot 10^{-11} \cdot e^{\frac{110}{T}}$
R24	$NO_2 + O_3 \rightarrow NO_3 + O_2$	$1.40 \cdot 10^{-13} \cdot e^{\frac{-2470}{T}}$
R25	$NO_2 + NO_3 \rightarrow N_2O_5$	**
R26	$N_2O_5 \rightarrow NO_3 + NO_2$	***
R27	$N_2O_5 + H_2O \rightarrow 2HNO_3$	$2.50 \cdot 10^{-22}$
R28	$N_2O_5 + 2H_2O \rightarrow 2HNO_3 + H_2O$	$1.80 \cdot 10^{-39}$
R29	$TERP + O_3 \rightarrow \alpha_1^T TC_1 + \alpha_2^T TC_2 \alpha_3^T TC_3 + \alpha_4^T TC_4$	$5.00 \cdot 10^{-16} \cdot e^{\frac{-570}{T}}$
R30	$TERP + OH \rightarrow \alpha_1^T TC_1 + \alpha_2^T TC_2 \alpha_3^T TC_3 + \alpha_4^T TC_4$	$1.21 \cdot 10^{-11} \cdot e^{\frac{436}{T}}$
R31	$OH + O_3 \rightarrow HO_2 + O_2$	$1.30 \cdot 10^{-12} \cdot exp\frac{-950}{T}$
R32	$ISOPOOH + OH \rightarrow IEPOX + OH$	$1.90 \cdot 10^{-11} \cdot exp\frac{390}{T}$
R33	$ISOPOOH + OH \rightarrow LVOC$	$1.7 \cdot 10^{-11}$
R34	$IEPOX + OH \rightarrow PRODUC$	$5.78 \cdot 10^{-11} \cdot exp\frac{-400}{T}$
R35	$LVOC \rightarrow 0.04ISOPOOH\text{-}SOA$	$6.6 \cdot 10^{-3} s^{-1}$
R36	$IEPOX \rightarrow 0.11IEPOX\text{-}SOA$	$1.54 \cdot 10^{-4} s^{-1}$

* $k = (k1 + k2)/k3; k1 = 2.21 \cdot 10^{-13} \cdot e^{\frac{600}{T}}; k2 = 1.91 \cdot 10^{-33} \cdot c_{air}; k3 = 1 + 1.4 \cdot 10^{-21} \cdot e^{\frac{2200}{T}} \cdot C_{H_2O}$

** $k = 0.35 \cdot (k_0 k_\infty)/(k_0 + k_\infty); k_0 = 3.61 \cdot 10^{-30} \cdot (\frac{T}{300})^{-4.1} \cdot c_{N_2}; k_\infty = 1.91 \cdot 10^{-12} \cdot (\frac{T}{300})^{0.2}$

*** $k = 0.35 \cdot (k_0 k_\infty)/(k_0 + k_\infty); k_0 = 1.31 \cdot 10^{-3} \cdot (\frac{T}{300})^{-3.5} \cdot e^{\frac{-11000}{T}} \cdot c_{N_2}; k_\infty = 9.71 \cdot 10^{14} \cdot (\frac{T}{300})^{0.1} \cdot e^{\frac{-11080}{T}}$

Land Surface Set Up

.2 Gamma factors - BVOC calculations

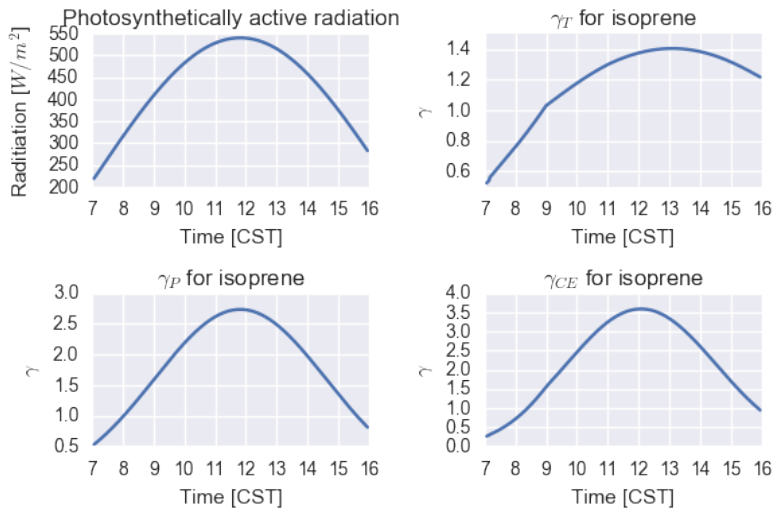

FIGURE 13: (a) The photosynthetically active radiation, (b) the temperature-dependent gamma factor (c) the light-dependent gamma factor and subsequent canopy environment gamma factor for isoprene emissions, calculated as per Guenther (2006).

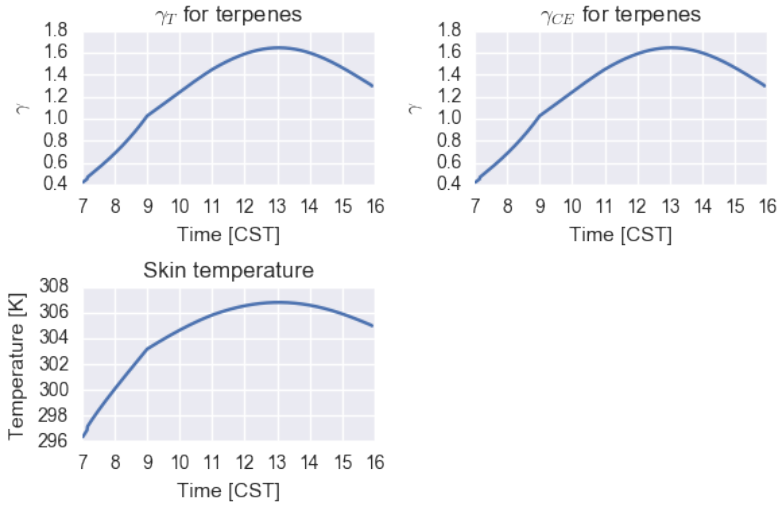

FIGURE 14: (a) The temperature-dependent gamma factor, (b) canopy environment gamma factor for terpene emissions and (c) the skin temperature, calculated as per Guenther (2006).

Figures

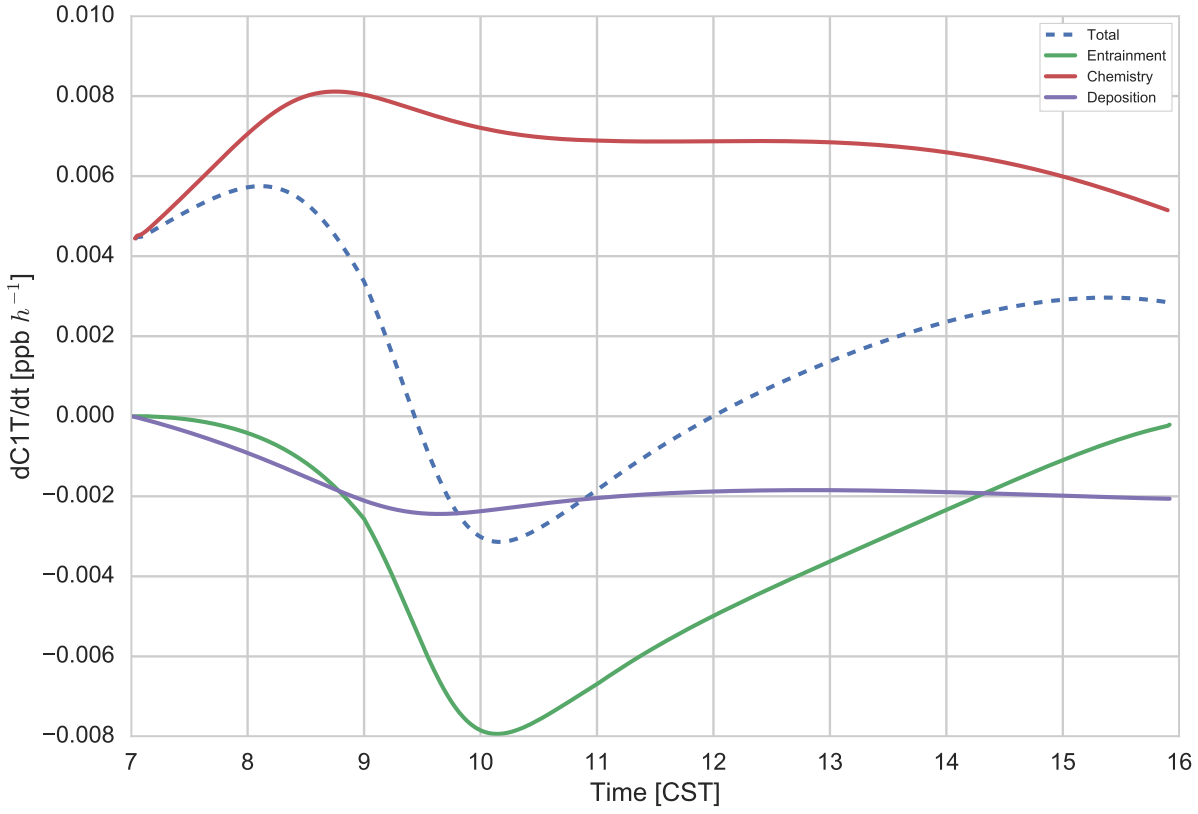

FIGURE 15: The monoterpene-derived semi-volatile organic compound (C1T) budget with the total tendency (dashed), contribution due to entrainment (green), contribution due to chemistry (red) and contribution due to deposition (purple).

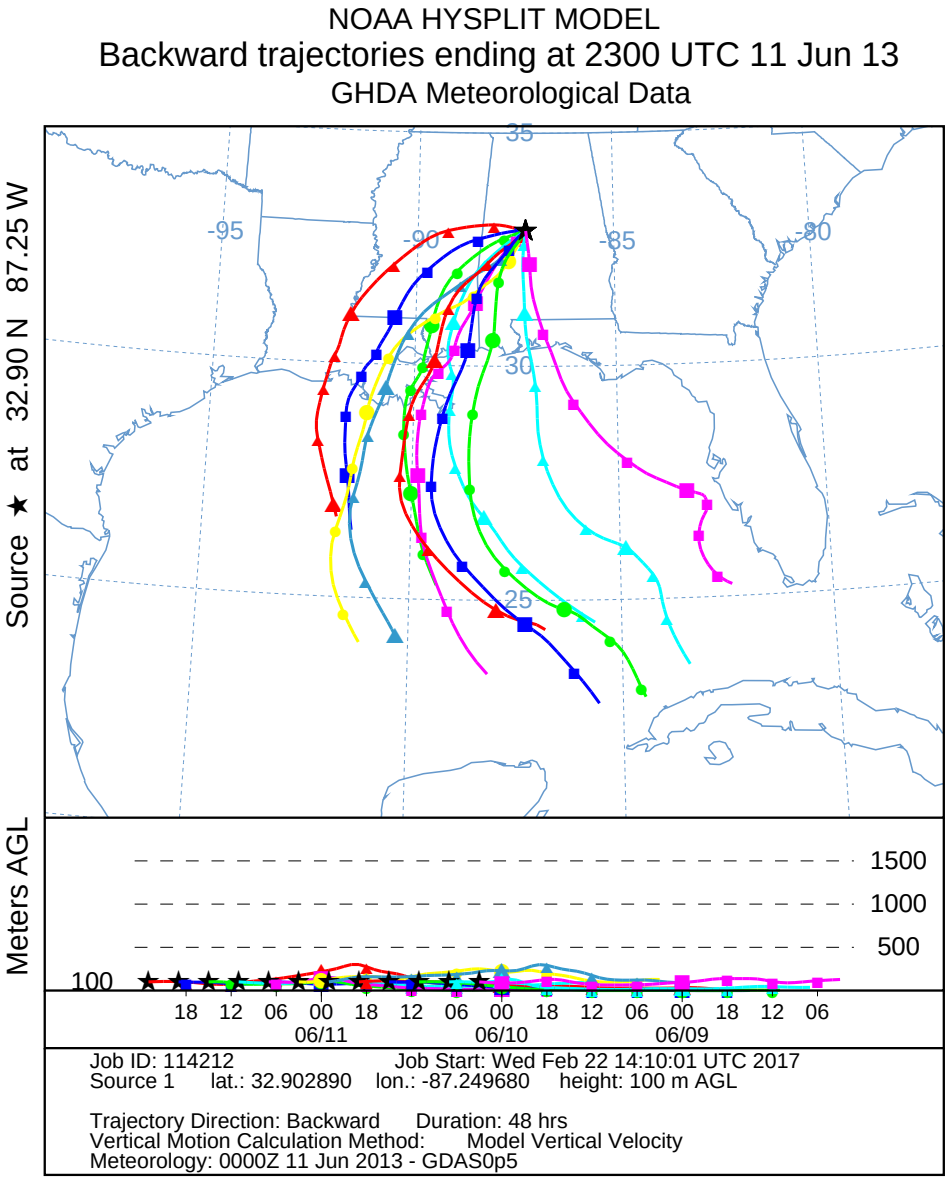

FIGURE 16: Backward air mass trajectories from 06:00 CST on June 6 to 23:00 CST on June 11 at 100 m, arriving at the SOAS measurement site in Centerville, Alabama from the NOAA Hysplit Trajectory Model.

Bibliography

Ahmadov, R., McKeen, S., Robinson, A., Bahreini, R., Middlebrook, A., Gouw, J. d., Meagher, J., Hsie, E.-Y., Edgerton, E., Shaw, S., et al. (2012). A volatility basis set model for summertime secondary organic aerosols over the eastern united states in 2006. *Journal of Geophysical Research: Atmospheres*, 117(D6).

Ayres, B. R., Allen, H. M., Draper, D. C., Brown, S. S., Wild, R. J., Jimenez, J. L., Day, D. A., Campuzano-Jost, P., Hu, W., De Gouw, J., Koss, A., Cohen, R. C., Duffey, K. C., Romer, P., Baumann, K., Edgerton, E., Takahama, S., Thornton, J. A., Lee, B. H., Lopez-Hilfiker, F. D., Mohr, C., Wennberg, P. O., Nguyen, T. B., Teng, A., Goldstein, A. H., Olson, K., and Fry, J. L. (2015). Organic nitrate aerosol formation via NO3+ biogenic volatile organic compounds in the southeastern United States. *Atmospheric Chemistry and Physics*, 15(23):13377–13392.

Barbaro, E., de Arellano, J. V.-G., Ouwersloot, H. G., Schröter, J. S., Donovan, D. P., and Krol, M. C. (2014). Aerosols in the convective boundary layer: Shortwave radiation effects on the coupled land-atmosphere system. *Journal of Geophysical Research: Atmospheres*, 119(10):5845–5863.

Bates, K. H., Crounse, J. D., St. Clair, J. M., Bennett, N. B., Nguyen, T. B., Seinfeld, J. H., Stoltz, B. M., and Wennberg, P. O. (2014). Gas phase production and loss of isoprene epoxydiols. *The Journal of Physical Chemistry A*, 118(7):1237–1246.

Bernard, P. S. and Wallace, J. M. (2002). *Turbulent flow: analysis, measurement, and prediction.* John Wiley & Sons.

Bessagnet, B., Seigneur, C., and Menut, L. (2010). Impact of dry deposition of semi-volatile organic compounds on secondary organic aerosols. *Atmospheric environment*, 44(14):1781–1787.

Budisulistiorini, S. H., Li, X., Bairai, S. T., Renfro, J., Liu, Y., Liu, Y. J., McKinney, K. A., Martin, S. T., McNeill, V. F., Pye, H. O. T., Nenes, A., Neff, M. E., Stone, E. A., Mueller, S., Knote, C., Shaw, S. L., Zhang, Z., Gold, A., and Surratt, J. D. (2015). Examining the effects of anthropogenic emissions on isoprene-derived secondary organic aerosol formation during

the 2013 Southern Oxidant and Aerosol Study (SOAS) at the Look Rock, Tennessee ground site. *Atmospheric Chemistry and Physics*, 15(15):8871–8888.

Canagaratna, M., Jayne, J., Jimenez, J., Allan, J., Alfarra, M., Zhang, Q., Onasch, T., Drewnick, F., Coe, H., Middlebrook, A., et al. (2007). Chemical and microphysical characterization of ambient aerosols with the aerodyne aerosol mass spectrometer. *Mass Spectrometry Reviews*, 26(2):185–222.

Carlton, A., de Gouw, J., Jimenez, J., Ambrose, J., Brown, S., Baker, K., Brock, C., Cohen, R., Edgerton, S., Farkas, C., et al. (2016). The southeast atmosphere studies (sas): Coordinated investigation and discovery to answer critical questions about fundamental atmospheric processes. *Bull. Amer. Meteor. Soc.*

Carlton, A., Wiedinmyer, C., and Kroll, J. (2009). A review of secondary organic aerosol (soa) formation from isoprene. *Atmospheric Chemistry and Physics*, 9(14):4987–5005.

DeCarlo, P. F., Kimmel, J. R., Trimborn, A., Northway, M. J., Jayne, J. T., Aiken, A. C., Gonin, M., Fuhrer, K., Horvath, T., Docherty, K. S., et al. (2006). Field-deployable, high-resolution, time-of-flight aerosol mass spectrometer. *Analytical chemistry*, 78(24):8281–8289.

Donahue, N., Robinson, A., Stanier, C., and Pandis, S. (2006). Coupled partitioning, dilution, and chemical aging of semivolatile organics. *Environmental Science & Technology*, 40(8):2635–2643.

Farmer, D. K., Chen, Q., Kimmel, J. R., Docherty, K. S., Nemitz, E., Artaxo, P. a., Cappa, C. D., Martin, S. T., and Jimenez, J. L. (2013). Chemically Resolved Particle Fluxes Over Tropical and Temperate Forests. *Aerosol Science and Technology*, 47(7):818–830.

Feingold, G., Jiang, H., and Harrington, J. Y. (2005). On smoke suppression of clouds in amazonia. *Geophysical Research Letters*, 32(2).

Field, R., Fritschen, L., Kanemasu, E., Smith, E., Stewart, J., Verma, S., and Kustas, W. (1992). Calibration, comparison, and correction of net radiation instruments used during fife. *Journal of Geophysical Research: Atmospheres*, 97(D17):18681–18695.

Froyd, K., Murphy, S., Murphy, D., De Gouw, J., Eddingsaas, N., and Wennberg, P. (2010). Contribution of isoprene-derived organosulfates to free tropospheric aerosol mass. *Proceedings of the National Academy of Sciences*, 107(50):21360–21365.

Gaston, C. J., Riedel, T. P., Zhang, Z., Gold, A., Surratt, J. D., and Thornton, J. A. (2014). Reactive uptake of an isoprene-derived epoxydiol to submicron aerosol particles. *Environmental Science and Technology*, 48(19):11178–11186.

Goldstein, A. H., Koven, C. D., Heald, C. L., and Fung, I. Y. (2009). Biogenic carbon and anthropogenic pollutants combine to form a cooling haze over the southeastern united states. *Proceedings of the National Academy of Sciences*, 106(22):8835–8840.

Guenther, A. (2006). Estimates of global terrestrial isoprene emissions using megan (model of emissions of gases and aerosols from nature). *Atmospheric Chemistry and Physics*, 6.

Guenther, A., Hewitt, C. N., Erickson, D., Fall, R., Geron, C., Graedel, T., Harley, P., Klinger, L., Lerdau, M., McKay, W., et al. (1995). A global model of natural volatile organic compound emissions. *Journal of Geophysical Research: Atmospheres*, 100(D5):8873–8892.

Guenther, A., Jiang, X., Heald, C., Sakulyanontvittaya, T., Duhl, T., Emmons, L., and Wang, X. (2012). The model of emissions of gases and aerosols from nature version 2.1 (megan2. 1): an extended and updated framework for modeling biogenic emissions.

Hidy, G. M., Blanchard, C. L., Baumann, K., Edgerton, E., Tanenbaum, S., Shaw, S., Knipping, E., Tombach, I., Jansen, J., and Walters, J. (2014). Chemical climatology of the southeastern United States, 1999–2013. *Atmospheric Chemistry and Physics*, 14(21):11893–11914.

Horn, G., Ouwersloot, H., De Arellano, J. V.-G., and Sikma, M. (2015). Cloud shading effects on characteristic boundary-layer length scales. *Boundary-Layer Meteorology*, 157(2):237–263.

Hu, W., Palm, B. B., Day, D. A., Campuzano-Jost, P., Krechmer, J. E., Peng, Z., De Sa Suzane, S., Martin, S. T., Alexander, M. L., Baumann, K., Hacker, L., Kiendler-Scharr, A., Koss, A. R., De Gouw, J. A., Goldstein, A. H., Seco, R., Sjostedt, S. J., Park, J. H., Guenther, A. B., Kim, S., Canonaco, F., Pr??v??t, A. S. H., Brune, W. H., and Jimenez, J. L. (2016). Volatility and lifetime against OH heterogeneous reaction of ambient isoprene-epoxydiols-derived secondary organic aerosol (IEPOX-SOA). *Atmospheric Chemistry and Physics*, 16(18):11563–11580.

Huang, R.-J., Zhang, Y., Bozzetti, C., Ho, K.-F., Cao, J.-J., Han, Y., Daellenbach, K. R., Slowik, J. G., Platt, S. M., Canonaco, F., et al. (2014). High secondary aerosol contribution to particulate pollution during haze events in china. *Nature*, 514(7521):218–222.

Janssen, R., Vilà-Guerau de Arellano, J., Ganzeveld, L., Kabat, P., Jimenez, J., Farmer, D., Van Heerwaarden, C., and Mammarella, I. (2012). Combined effects of surface conditions, boundary layer dynamics and chemistry on diurnal soa evolution. *Atmospheric Chemistry and Physics*, 12(15):6827–6843.

Janssen, R., Vilà-Guerau de Arellano, J., Jimenez, J., Ganzeveld, L., Robinson, N., Allan, J., Coe, H., and Pugh, T. (2013). Influence of boundary layer dynamics and isoprene chemistry on

the organic aerosol budget in a tropical forest. *Journal of Geophysical Research: Atmospheres*, 118(16):9351–9366.

Jimenez, J., Canagaratna, M., Donahue, N., Prevot, A., Zhang, Q., Kroll, J. H., DeCarlo, P. F., Allan, J. D., Coe, H., Ng, N., et al. (2009). Evolution of organic aerosols in the atmosphere. *Science*, 326(5959):1525–1529.

Karl, T., Guenther, A., Turnipseed, A., Tyndall, G., Artaxo, P., and Martin, S. (2009). Rapid formation of isoprene photo-oxidation products observed in amazonia. *Atmospheric Chemistry and Physics*, 9(20):7753–7767.

Karl, T., Guenther, A., Yokelson, R. J., Greenberg, J., Potosnak, M., Blake, D. R., and Artaxo, P. (2007). The tropical forest and fire emissions experiment: Emission, chemistry, and transport of biogenic volatile organic compounds in the lower atmosphere over amazonia. *Journal of Geophysical Research: Atmospheres*, 112(D18).

Krechmer, J. E., Coggon, M. M., Massoli, P., Nguyen, T. B., Crounse, J. D., Hu, W., Day, D. A., Tyndall, G. S., Henze, D. K., Rivera-Rios, J. C., Nowak, J. B., Kimmel, J. R., Mauldin, R. L., Stark, H., Jayne, J. T., Sipil??, M., Junninen, H., St. Clair, J. M., Zhang, X., Feiner, P. A., Zhang, L., Miller, D. O., Brune, W. H., Keutsch, F. N., Wennberg, P. O., Seinfeld, J. H., Worsnop, D. R., Jimenez, J. L., and Canagaratna, M. R. (2015). Formation of Low Volatility Organic Compounds and Secondary Organic Aerosol from Isoprene Hydroxyhydroperoxide Low-NO Oxidation. *Environmental Science and Technology*, 49(17):10330–10339.

Lane, T. E., Donahue, N. M., and Pandis, S. N. (2008). Simulating secondary organic aerosol formation using the volatility basis-set approach in a chemical transport model. *Atmospheric Environment*, 42(32):7439–7451.

Li, X., Rohrer, F., Hofzumahaus, A., Brauers, T., Häseler, R., Bohn, B., Broch, S., Fuchs, H., Gomm, S., Holland, F., et al. (2014). Missing gas-phase source of hono inferred from zeppelin measurements in the troposphere. *Science*, 344(6181):292–296.

Lilly, D. K. (1968). Models of cloud-topped mixed layers under a strong inversion. *Quarterly Journal of the Royal Meteorological Society*, 94(401):292–309.

Lin, Y.-H., Knipping, E., Edgerton, E., Shaw, S., and Surratt, J. D. (2013). Investigating the influences of so 2 and nh 3 levels on isoprene-derived secondary organic aerosol formation using conditional sampling approaches. *Atmospheric Chemistry and Physics*, 13(16):8457–8470.

Lopez-Hilfiker, F. D., Mohr, C., D'Ambro, E. L., Lutz, A., Riedel, T. P., Gaston, C. J., Iyer, S., Zhang, Z., Gold, A., Surratt, J. D., Lee, B. H., Kurten, T., Hu, W. W., Jimenez, J., Hallquist, M., and Thornton, J. A. (2016). Molecular Composition and Volatility of Organic Aerosol

in the Southeastern U.S.: Implications for IEPOX Derived SOA. *Environmental Science and Technology*, 50(5).

Mauderly, J. L. and Chow, J. C. (2008). Health effects of organic aerosols. *Inhalation toxicology*, 20(3):257–288.

Murphy, D., Cziczo, D., Froyd, K., Hudson, P., Matthew, B., Middlebrook, A., Peltier, R. E., Sullivan, A., Thomson, D., and Weber, R. (2006). Single-particle mass spectrometry of tropospheric aerosol particles. *Journal of Geophysical Research: Atmospheres*, 111(D23).

Nguyen, T. B., Bates, K. H., Crounse, J. D., Schwantes, R. H., Zhang, X., Kjaergaard, H. G., Surratt, J. D., Lin, P., Laskin, A., Seinfeld, J. H., and Wennberg, P. O. (2015a). Mechanism of the hydroxyl radical oxidation of methacryloyl peroxynitrate (MPAN) and its pathway toward secondary organic aerosol formation in the atmosphere. *Phys. Chem. Chem. Phys.*, 17(27):17914–17926.

Nguyen, T. B., Crounse, J. D., Teng, A. P., Clair, J. M. S., Paulot, F., Wolfe, G. M., and Wennberg, P. O. (2015b). Rapid deposition of oxidized biogenic compounds to a temperate forest. *Proceedings of the National Academy of Sciences*, 112(5):E392–E401.

Novakov, T. and Penner, J. (1993). Large contribution of organic aerosols to cloud-condensation-nuclei concentrations.

Ouwersloot, H., Arellano, J., H van Stratum, B., Krol, M., and Lelieveld, J. (2013). Quantifying the transport of subcloud layer reactants by shallow cumulus clouds over the amazon. *Journal of Geophysical Research: Atmospheres*, 118(23).

Paulot, F., Crounse, J. D., Kjaergaard, H. G., Kürten, A., Clair, J. M. S., Seinfeld, J. H., and Wennberg, P. O. (2009). Unexpected epoxide formation in the gas-phase photooxidation of isoprene. *Science*, 325(5941):730–733.

Sakulyanontvittaya, T., Duhl, T., Wiedinmyer, C., Helmig, D., Matsunaga, S., Potosnak, M., Milford, J., and Guenther, A. (2008). Monoterpene and sesquiterpene emission estimates for the united states. *Environmental science & technology*, 42(5):1623–1629.

Sillman, S., Logan, J. A., and Wofsy, S. C. (1990). The sensitivity of ozone to nitrogen oxides and hydrocarbons in regional ozone episodes. *Journal of Geophysical Research: Atmospheres*, 95(D2):1837–1851.

Situ, S., Wang, X., Guenther, A., Zhang, Y., Wang, X., Huang, M., Fan, Q., and Xiong, Z. (2014). Uncertainties of isoprene emissions in the megan model estimated for a coniferous and broad-leaved mixed forest in southern china. *Atmospheric Environment*, 98:105–110.

Stocker, T. F., Qin, D., Plattner, G.-K., T., B., M. M., Allen, S. K., Boschung, J., Nauels, A., Xia, Y., Bex, V., and Midgley, P. M., editors (2013). *Climate Change 2013: The Physical Science Basis, Working Group I Contribution to the Fifth Assessment Report of the Intergovernmental Panel on Climate Change*. Cambridge University Press.

Stull, R. (1988). An introduction to boundary layer meteorology kluwer academic publishers dordrecht 666 google scholar.

Su, L., Patton, E. G., De Arellano, J. V. G., Guenther, A. B., Kaser, L., Yuan, B., Xiong, F., Shepson, P. B., Zhang, L., Miller, D. O., Brune, W. H., Baumann, K., Edgerton, E., Weinheimer, A., Misztal, P. K., Park, J. H., Goldstein, A. H., Skog, K. M., Keutsch, F. N., and Mak, J. E. (2016). Understanding isoprene photooxidation using observations and modeling over a subtropical forest in the southeastern US. *Atmospheric Chemistry and Physics*, 16(12):7725–7741.

Takekawa, H., Minoura, H., and Yamazaki, S. (2003). Temperature dependence of secondary organic aerosol formation by photo-oxidation of hydrocarbons. *Atmospheric Environment*, 37(24):3413–3424.

Tennekes, H. (1973). A model for the dynamics of the inversion above a convective boundary layer. *Journal of the atmospheric sciences*, 30(4):558–567.

Tennekes, H. and Driedonks, A. (1981). Basic entrainment equations for the atmospheric boundary layer. *Boundary-Layer Meteorology*, 20(4):515–531.

Trainer, M., Williams, E. J., Parrish, D., Buhr, M., Allwine, E., Westberg, H., Fehsenfeld, F. C., and Liu, S. C. (1987). Models and observations of the impact of natural hydrocarbons on rural ozone. *Nature*, 329:705–707.

Van Heerwaarden, C. C., Vilà-Guerau de Arellano, J., Moene, A. F., and Holtslag, A. A. (2009). Interactions between dry-air entrainment, surface evaporation and convective boundary-layer development. *Quarterly Journal of the Royal Meteorological Society*, 135(642):1277–1291.

van Stratum, B. J., Vilá-Guerau de Arellano, J., van Heerwaarden, C. C., and Ouwersloot, H. G. (2014). Subcloud-layer feedbacks driven by the mass flux of shallow cumulus convection over land. *Journal of the Atmospheric Sciences*, 71(3):881–895.

Vilà-Guerau de Arellano, J., Dries, K., and Pino, D. (2009). On inferring isoprene emission surface flux from atmospheric boundary layer concentration measurements. *Atmospheric Chemistry and Physics*, 9(11):3629–3640.

Vilà-Guerau de Arellano, J., Patton, E. G., Karl, T., van den Dries, K., Barth, M. C., and Orlando, J. J. (2011). The role of boundary layer dynamics on the diurnal evolution of

isoprene and the hydroxyl radical over tropical forests. *Journal of Geophysical Research: Atmospheres*, 116(D7).

Vilà-Guerau de Arellano, J., van Heerwaarden, C. C., van Stratum, B. J., and van den Dries, K. (2015). *Atmospheric boundary layer: Integrating air chemistry and land interactions*. Cambridge University Press.

Wagner, N., Brock, C., Angevine, W., Beyersdorf, A., Campuzano-Jost, P., Day, D., de Gouw, J., Diskin, G., Gordon, T., Graus, M., et al. (2015). In situ vertical profiles of aerosol extinction, mass, and composition over the southeast united states during senex and seac 4 rs: observations of a modest aerosol enhancement aloft. *Atmospheric Chemistry and Physics*, 15(12):7085–7102.

Wang, P., Schade, G., Estes, M., and Ying, Q. (2017). Improved megan predictions of biogenic isoprene in the contiguous united states. *Atmospheric Environment*, 148:337–351.

Washenfelder, R., Attwood, A., Brock, C., Guo, H., Xu, L., Weber, R., Ng, N., Allen, H., Ayres, B., Baumann, K., et al. (2015). Biomass burning dominates brown carbon absorption in the rural southeastern united states. *Geophysical Research Letters*, 42(2):653–664.

Weaver, H. L. (1990). Temperature and humidity flux-variance relations determined by one-dimensional eddy correlation. *Boundary-Layer Meteorology*, 53(1-2):77–91.

Xu, L., Guo, H., Boyd, C. M., Bougiatioti, A., Cerully, K. M., Hite, J. R., Isaacman-vanwertz, G., Kreisberg, N. M., Olson, K., Koss, A., Goldstein, A. H., Susanne, V., Gouw, J. D., Baumann, K., Lee, S.-h., Nenes, A., Weber, R. J., and Ng, N. L. (2015a). Correction for Xu et al., Effects of anthropogenic emissions on aerosol formation from isoprene and monoterpenes in the southeastern United States. *Proceedings of the National Academy of Sciences*, 112(32):201512277.

Xu, L., Guo, H., Boyd, C. M., Klein, M., Bougiatioti, A., Cerully, K. M., Hite, J. R., Isaacman-VanWertz, G., Kreisberg, N. M., Knote, C., et al. (2015b). Effects of anthropogenic emissions on aerosol formation from isoprene and monoterpenes in the southeastern united states. *Proceedings of the National Academy of Sciences*, 112(1):37–42.